NASA

Technical Memorandum **86214**

FAST AND OPTIMAL SOLUTION TO THE 'RANKINE-HUGONIOT PROBLEM'

Adolfo F. Viñas
Jack D. Scudder

MAY 1985

National Aeronautics and
Space Administration

Goddard Space Flight Center
Greenbelt, Maryland 20771

TM-86214

FAST AND OPTIMAL SOLUTION TO THE 'RANKINE-HUGONIOT PROBLEM'

Adolfo F. Viñas

and

Jack D. Scudder

Laboratory For Extraterrestrial Physics

NASA/Goddard Space Flight Center

Greenbelt, MD. 20771

Submitted to: Journal of Geophysical Research

Abstract

A new, definitive, reliable and fast iterative method is described for determining the geometrical properties of a shock (i. e. Θ_{Bn}, $\vec{n}$, V_s and M_A), the conservation constants and the self-consistent asymptotic magnetofluid variables, that uses the three dimensional magnetic field and plasma observations. The method is well conditioned and reliable at all Θ_{Bn} angles regardless of the shock strength or geometry. Explicit proof of 'uniqueness' of the shock geometry solution by either analytical or graphical methods is given. The method is applied to synthetic and real shocks, including a bow shock event and the results are then compared with those determined by preaveraging methods and other iterative schemes. A complete analysis of the confidence region and error bounds of the solution is also presented.

1. Introduction

The identification of an observed discontinuity as a shock rests on certifying a sequence of conditions (described below) which can only be rigorously expressed by specifying the geometrical orientation and speed of propagation of the discontinuity [Burlaga, 1971; Greenstadt et al., 1984]. Within the various classes of shocks, there are diverse geometrical, theoretical and observational regimes which further differentiate shocks into quasi-perpendicular versus quasi-parallel, subcritical versus supercritical, laminar versus turbulent and resistive versus dispersive [Greenstadt et al., 1984; Edminston and Kennel, 1985; Kennel et al., 1985]. To specify which of these shock regimes a given set of observations illustrates is the initial task for the increasingly quantitative shock studies made possibly by the ISEE and Voyager instrumentation. Furthermore, the importance of the shock geometry in relation to the origin of particle reflection and acceleration of thermal particles near shocks has been emphasized by Sonnerup [1969], Gosling et al. [1982], Armstrong et al. [1985], Forman and Webb [1985], Wu [1984] and Goodrich and Scudder [1984] among others. Direct spacecraft measurements only determine these geometrical properties implicitly; they must be empirically inferred by solving what we shall describe below as the "Rankine-Hugoniot (RH) problem". This problem consists of taking the spacecraft observations (or time series) of density, velocity and magnetic field across a shock and finding a suitable Galilean frame where the discontinuity is time-stationary and where defensibly conserved quantities can be defined such as the normal mass flux, tangential stress, normal component of the magnetic field and tangential electric field together with the upstream and downstream asymptotic

magnetofluid states. The solution of the RH problem is a non-trivial problem involving specifying eleven, non-linearly intertwined, free variables. The angle of shock propagation θ_{Bn} relative to the asymptotic upstream magnetic field $\vec{B}$ and the strength of the discontinuity characterized by the various Mach numbers can only be obtained after this frame shift, conservation constants and asymptotic states are determined. Once such a frame shift and states are found, a sequence of supplementary tests can be performed to determine if the discontinuity is a shock. In many respects it is easier to deny that a discontinuity is a shock than to guarantee that it is one.

The single spacecraft determination of shock normals on planetary and interplanetary shocks have been previously studied by Colburn and Sonnett [1966], Chao [1970], Lepping and Argentiero [1971], Lepping [1972], Abraham-Shrauner [1972], Abraham-Shrauner and Yun [1976], Chao and Hsieh [1984] and Acuña and Lepping [1984] among others. Four basic methods of single spacecraft shock normal determination are widely used. These are magnetic coplanarity (MC), velocity coplanarity (VC), the least squares method of Lepping and Argentiero (LA) and the mixed data methods of Abraham-Shrauner (AS). All these methods use a subset of the RH conservation equations. The subset of the RH equations that restate conservation of mass flux, normal component of the magnetic field, tangential component of the momentum flux and tangential component of the electric field do not discriminate between four MHD discontinuous classes such as contact discontinuity, rotational discontinuity, tangential discontinuity and shock. Except for the Lepping and Argentiero method and the procedure described in this paper, the other approaches have used an even smaller subset of the above set to estimate the shock normal, speed and

geometry. These different methods have often revealed disparate results in the shock parameters estimated for the same set of observations. One of the difficulties on relying in some of these methods is that their use requires that one predefine the asymptotic magnetofluid variables by an "ad hoc" pre-averaging procedure. It is not clear in the presence of waves or random fluctuations that this kind of "ad hoc" procedure can describe the self-consistent asymptotic states of a shock. Alternatively, iterative schemes such as the LA method have tried to resolve this problem by solving directly for the asymptotic magnetofluid variables. These variables are subsequently used together with the magnetic coplanarity and mass flux conservation expressions to determine the shock normal and speed. Although, this approach is self-consistent, the LA method has the unfortunate difficulty that its 11-dimensional space of unknown magnetofluid variables (ρ_1, ρ_2, $\vec{V}_2 - \vec{V}_1$, $\vec{B}_1$ and $\vec{B}_2$), which span the parameter space, is large and irreducible. Besides, this 11-dimensional space of variables is highly non-linear, giving rise for concern of the 'uniqueness' of the selected solution. Up to the present time, the problem of 'uniqueness' of the solution determined has remained completely unaddressed. Notice that methods that preaverage the data obviate questions of uniqueness by de facto algebraic computation.

Another method used in the estimation of shock parameters has been the use of observations from two or more spacecraft [Chao, 1970; Ogilvie and Burlaga, 1969; Russell et al., 1983a,b]. Since situations where shock observations at more than one spacecraft are uncommon, we shall limit our discussion to comparisons with single spacecraft methods. In the situation where such observations are available we shall report the results of parameters determined from such multiple spacecraft methods.

This paper presents a new, fast iterative approach and solution to the RH problem to determine the shock parameters by means of a non-linear least squares method. An essential concept of this new method is that there exist a simple set of 'natural' variables that is separable. The new set of variables (ϕ, θ, V_s, G_n, B_n, $\tilde{S}_t$, $\tilde{E}_t$, ρ_1 and ρ_2) together with two constraint equations form a vector basis that spans the 11 dimensional space of unknown parameters to be determined. By the term 'natural' we mean that choice of variables for which 'uniqueness' (or lack thereof) of the selected value is demonstrable either analytically (for linear variables) or graphically (for non-linear variables). Similarly, by separable we mean that the full set of 'natural' variables can be obtained through a self-consistent sequence of least squares problems each of which contains a small dimensional subspace (i. e. less than 2) of the complete set of unknown parameters. The existence of such an ordered sequence of smaller dimensional problems is a consequence of the fact that the RH equations which represent the model can be written in various forms permitting some of the unknown parameters to appear either explicitly or implicitly in the equations for the same set of observations. A further advantage of this approach over previous methods is that the number of linear variables of the unknown parameter space is large (i. e. seven) resulting in only four non-linear parameters of the full 11 dimensional space which require graphical 'uniqueness' investigation. By virtue of this separability we can explore the 'uniqueness' (or lack thereof) of all the possible minima that encompasses the optimal solutions of the RH equations. It is clear that the set of RH equations can support in addition to the shock solution other types of discontinuous solutions such as rotational, tangential and contact discontinuities which are inherent to the system of equations [Landau and

Lifshitz, 1960; Burlaga, 1971; Akhiezer et al., 1975]. After a thorough inspection of each of these minima and using a series of supplementary tests we can determine the most likely physical shock solution (if it exists) to the problem. Among the necessary conditions that an observed discontinuity must satisfy to be identified as a possible shock are: a)that in the selected Galilean frame, there should exist a defensibly non-vanishing mass flux, b)that there is a density and total electron plus ion temperature (if available) jump in the same sense across the discontinuity, c)that there should be a decrease of the normal component of the fluid velocity in the direction the density increases and c)that the predicted thermal normal pressure must increase with the density and should be comparable within the noise with the observed pressure (if available).

In addition to providing explicit proofs of 'uniqueness' (or lack thereof), the method converges equally fast for quasi-parallel or quasi-perpendicular shocks (for which extant methods converge extremely slowly requiring one/half day of VAX 11/780 computing time to determine a solution). This new approach rarely takes more than a few seconds of computing time to correctly determine the shock parameters, the Rankine-Hugoniot conservation constants, as well as to graphically support the 'uniqueness' of the shock geometry selected. The method uses the observed plasma velocity and density as well as magnetic field measurements on both sides of the observed shock. The sequence of problems consists of initially determining the shock normal polar angles (ϕ, θ) and the shock speed V_s using the Rankine-Hugoniot equations and the plasma and magnetic field data given by ρ, $\vec{V}$ and $\vec{B}$ on both sides of the shock by a non-linear least squares method. Once the optimal shock normal angles and speed have been determined , their values are used in conjunction with the data to

uniquely define the conserved constants. These constants are the mass flux G_n, the normal component of the magnetic field B_n, the tangential components of the momentum flux $\overset{+}{S}_t$ and the tangential components of the electric field $\overset{+}{E}_t$ in the frame of the observations. Finally, we use the determined shock normal, speed and conservation constants in conjuntion with the data back in the RH equations to predict the self-consistent asymptotic states of the magnetofluid in the upstream and downstream sides of the shock. We also estimate the error bounds and the region of confidence for the shock parameters.

This paper is organized in the following manner. Section 2 presents a brief description of the RH conservation equations and their representation in an arbitrary reference system. The separable sequence of the least squares scheme for the solution of the shock geometry is presented in section 3. In section 4 we discuss the applications and results of this approach on simulated and real shocks. The results are then compared with those obtained by different techniques. Finally, a summary and conclusions of the results obtained is presented in section 5, with possible suggestions for future work.

2. Rankine-Hugoniot Conservation Equations: The Model

The determination scheme for the shock normal, shock speed, conservation constants and asymptotic states rests on a series of assumptions: 1)these parameters can be determined from the model equations of the Rankine-Hugoniot system; 2)there exist such a frame in which the shock is time-stationary; 3)the observations used in their determination constitute an ensemble of asymptotic states as predicted by the conservations

equations. This last assumption means that we are able to remove information associated with the shock (transition) layer.

The conservations equations evaluated in the shock frame of reference (represented here by asterisk) for an isotropic plasma medium are [Boyd and Sanderson, 1969]:

$$\Delta[\ \rho V_n^{*}\ ] = 0 \tag{1}$$

$$\Delta[\ \rho V_n^{*}\ \vec{V}_t^{*} - \frac{B_n \vec{B}_t}{4\pi}\ ] = 0 \tag{2}$$

$$\Delta[\ B_n\ (\vec{n} \times \vec{V}_t^{*}) - V_n^{*}\ (\vec{n} \times \vec{B}_t)\ \ ] = 0 \tag{3}$$

$$\Delta[\ \vec{B} \cdot \vec{n}\ ] = 0 \tag{4}$$

$$\Delta[\ P + \frac{(B^2 - B_n^{\,2})}{8\pi} + \rho V_n^{*2}\ ] = 0 \tag{5}$$

$$\Delta[\ \rho V_n^{*}\ \frac{V^{*2}}{2} + \rho V_n^{*}\ (\ \frac{\gamma}{(\gamma-1)}\ \frac{P}{\rho} + \frac{B^2}{4\pi\rho}\ ) - \frac{B_n(\vec{V}^{*} \cdot \vec{B})}{4\pi}\ ] = 0 \tag{6}$$

where ρ is the plasma mass density, V_n^{*} is the plasma bulk velocity component along the normal to the shock surface, $\vec{V}_t^{*}$ is the flow velocity tangential to the shock surface, B_n and $\vec{B}_t$ are the associated normal and tangential components of the magnetic field, P is the total kinetic pressure, $\vec{n}$ is the normal unit vector and γ is the adiabatic constant. The subscripts n and t imply projection operators defined for any vector $\vec{A}$ as $A_n = \vec{A} \cdot \vec{n}$ and $\vec{A}_t = \vec{A} \cdot (\underline{\underline{I}} - \vec{n}\vec{n})$ where $\underline{\underline{I}}$ is the unit tensor. The symbol Δ means that the quantity within brackets is to be evaluated after ('2') and before ('1')

the shock transition layer as indicated by the time arrow and then substracted (i. e. $\Delta\Psi = \Psi_2 - \Psi_1$). Equation (1) represents the mass flux conservation equation, (2) is the momentum flux conservation equation for the tangential components, (3) is the continuity equation for the tangential electric field, (4) is the continuity of the normal component of the magnetic field, (5) is the conservation of the normal momentum flux and finally, (6) is the energy flux conservation equation. Note that $\vec{B} = \vec{B}^*$ for a Galilean frame shift. If the plasma is anisotropic, equations (5) and (6) will change. In general the normal pressure term in (5) is represented by $\vec{n}\cdot\underline{\underline{P}}\cdot\vec{n}$ where $\underline{\underline{P}}$ is the full pressure tensor. However for an isotropic plasma, the tensor is diagonal and the expression $\vec{n}\cdot\underline{\underline{P}}\cdot\vec{n}$ reduces to P. These system of equations can be simply expressed by means of a Galilean transformation into an arbitrary frame of reference (as for example the one where the observations are made) by the transformation

$$\vec{V} = \vec{V}^* + \vec{V}_s \tag{7}$$

where $\vec{V}_s = V_s \vec{n}$ represents the shock velocity and $\vec{V}$ is the plasma flow velocity in the frame of reference of the observations.

It is clear from looking at these equations that they cannot be used without knowledge of the shock normal $\vec{n}$, the shock speed V_s as well as the quantities ρ, $\vec{V}$, $\vec{B}$, P and the constant γ on each side of the shock. Equations (5) and (6) will not be used in our calculations. Although in some experiments the total kinetic pressure tensor (i. e. electron plus ion pressure) is known and in principle equation (5) could be used, this is not always so in all cases. Furthermore, in order for us to make a fair comparison of our method with others such as for example the LA method, we

shall restrict our system of conservation equations to (1) - (4) since they are statements of proper conservation quantities within the approximation $E^2 << B^2$.

The Rankine-Hugoniot equations (1) - (4) writen in an arbitrary reference system using (7) are:

$$\Delta[G_n] = \Delta[\rho(\vec{V} - V_s \vec{n}) \cdot \vec{n}] = 0 \tag{8}$$

$$\Delta[B_n] = \Delta[\vec{B} \cdot \vec{n}] = 0 \tag{9}$$

$$\Delta[\vec{S}_t] = \Delta[\rho(\vec{V} \cdot \vec{n} - V_s)\ (\vec{V}\cdot(\underline{\underline{I}}-\vec{n}\vec{n})) - \frac{(\vec{B}\cdot\vec{n})}{4\pi}\ (\vec{B}\cdot(\underline{\underline{I}}-\vec{n}\vec{n}))\ ] = 0 \tag{10}$$

$$\Delta[\vec{E}_t] = \Delta[\ \vec{n} \times (\vec{V}\cdot(\underline{\underline{I}}-\vec{n}\vec{n}))\ (\vec{B}\cdot\vec{n}) - (\vec{V}\cdot\vec{n} - V_s)\ \vec{n} \times (\vec{B}\cdot(\underline{\underline{I}}-\vec{n}\vec{n}))\ ] = 0 \tag{11}$$

where we have used $V_n^* = (\vec{V} - V_s\vec{n})\cdot\vec{n}$ and $\vec{V}_t^* = \vec{V}_t$ since $\vec{V}_s\cdot(\underline{\underline{I}}-\vec{n}\vec{n})$ vanishes in any arbitrary frame of reference. The variables G_n, B_n, $\vec{S}_t$ and $\vec{E}_t$ represent the conservation constants corresponding to mass flux, normal magnetic field, tangential momentum flux (stress) and tangential electric field, respectively. These equations represent a system of eight equations since (10) and (11) are vectorial expressions in an arbitrary system. In our notation the vector $\vec{n} = (n_x, n_y, n_z)$ can be expressed in any orthonormal system of coordinates where the observations are made, e. g. the heliocentric coordinate system (R, T, N). In addition to these equations we also have the normalization condition

$$|\vec{n}| = 1$$

which acts as a constraint equation and allow us to reduce the space of

unknown parameters by one variable. This is accomplished by expressing the normal components in spherical coordinates as

$$\begin{aligned} n_x &= \cos\theta \\ n_y &= \cos\phi \sin\theta \qquad \text{where } 0 \leq \phi \leq 2\pi, \text{ and } 0 \leq \theta \leq \pi \\ n_z &= \sin\phi \sin\theta \end{aligned} \tag{12}$$

Generally this selection of the sense of the shock normal direction is arbitrary. With these conditions the variables of the system are the two angles (ϕ, θ), the shock speed V_s and the magnetic field and plasma parameters. This final set of eight equations forms the basic system of equations that we use to determine the shock geometry by least squares.

3. Application of the Sequence Method to the Rankine-Hugoniot Problem

In this section we shall present the sequence of least squares problems that are used to determine the shock geometry using the model equations (8) - (11) described above. The basic RH problem can be stated as follows: given a typical ensemble of observations (i. e. a time series) of density ρ, velocity $\vec{V}$ and magnetic field $\vec{B}$ with random noise and/or waves superposed, characterizing disturbed states about a possible asymptotic (undisturbed) states and about a discontinuous change in fluid variables, estimate the optimal shock normal, shock speed, the conserved quantities across the shock and the appropriate compatible combination of magnetofluid variables that characterizes the self-consistent asymptotic states of the observed discontinuity. As initially posed, this problem requires the solution in an 11-dimensional space. In the subsequent sections it is shown that we can

reduce this multidimensional problem to a self-consistent sequence of least squares problems of smaller dimensions (i. e. less than or equal 2) each of which has a solution that can be demonstrated to be optimal, if not 'unique'.

a. Shock normal and speed determination

The first problem in the sequence is the calculation of the shock normal $\vec{n}$ and the shock speed V_s using equations (8) - (11) and the observations of density, velocity and magnetic field at both sides of the shock. We use a further simplification of the system of equations (8) - (11) by solving for the shock speed V_s in equation (8) since it enters linearly in the equation. From equation (8) we get

$$V_s = \frac{\Delta[\rho\vec{V}]}{\Delta[\rho]} \cdot \vec{n} \qquad (13)$$

which is the usual form for the shock speed. Substituting (13) into (9)-(11) we get a system of seven equations in terms of density ρ, velocity $\vec{V}$, magnetic field $\vec{B}$ and the shock normal polar angles (ϕ, θ). If we now let the density, velocity and magnetic field to be given by the observations, then the final set of seven equations only contains two unknown parameters (ϕ, θ). In our notation we define the model function $\vec{F}'(\vec{x}; \vec{p}) = 0$ as a vector of seven components formed by the final derived expressions. We also define the vectors $\vec{x} = (\rho_1, \vec{V}_1, \vec{B}_1, \rho_2, \vec{V}_2, \vec{B}_2)$ and $\vec{p} = (\phi, \theta)$ to represent the observations at both sides of the shock and the unknown parameters to be determined, respectively. Since $\vec{F}'(\vec{x}; \vec{p})$ is a vector formed by the seven RH equations and we have a set of N pairs (i. e. both sides) of observations we now define a vector function $\vec{F}(\vec{x}; \vec{p}) = \{ \vec{F}_i'(\vec{x}_i; \vec{p}) \}$ of size $N' = 7 \times N$

which is the model function that represents all the observations since the index i varies fron one to N. The function $\vec{F}(\vec{x};\ \vec{p})$ can be expanded locally in Taylor series about some initial parameter set $\vec{p}^{(o)} = (\phi^{(o)},\ \theta^{(o)})$ as

$$\vec{Y} = \vec{F}(\vec{x};\ \vec{p}^{(o)}) + \left.\frac{\partial \vec{F}}{\partial \vec{p}}\right|_{\vec{p}\,(o)} \Delta\vec{p} + \ldots \tag{14}$$

Equation (14) can be expressed in matrix notation as follows

$$\underline{\underline{A}}\ \Delta\vec{p} = \Delta\vec{Y} \tag{15}$$

where $\Delta\vec{Y} = \vec{Y} - \vec{F}(\vec{x};\ \vec{p}^{(o)})$ is a vector of length N' where $\vec{Y}$ is the null vector (i. e. $Y_i = 0,\ i = 1,\ N'$) indicating that the conservation equations must be satisfied exactly. Equation (15) is called the normal equation of least squares. In this equation we also have defined $\underline{\underline{A}}$ as a matrix of size N' x M (where M=2 the number of unknown parameters) formed by the partial derivatives of the seven model Rankine-Hugoniot equations with respect to the unknown parameters $\vec{p} = (\phi,\ \theta)$ evaluated at the initial guess. These derivatives have been evaluated analytically and verified by numerical integration.

For the sake of simplicity, we shall present the details of the least squares methodology of the solution of equation (15) in Appendix A. However, to summarize the results, the final solution of this equation is obtained by an iterative scheme that minimizes the norm of the residuals or the variance $\chi^2(\phi,\ \theta) = \vec{r}^{\,T}\ \vec{r}$ where $\vec{r} = (\underline{\underline{A}}\ \Delta\vec{p} - \Delta\vec{Y})$. Once this minimum has been obtained the optimal solution $\vec{p}^{\,*} = \vec{p} + \Delta\vec{p}$ is recovered. From this optimal solution $\vec{p}^{\,*} = (\phi^*,\ \theta^*)$ we can now recover the normal $\vec{n}$ using equation (12). We can easily demonstrate by graphical methods the

'uniqueness' of the solution $\vec{p}^{*} = (\phi^{*}, \theta^{*})$ because there are only two free parameters. In this circumstance we can construct a plot of the contours of the $\log\chi^2(\theta, \phi)$ function versus the angles θ and ϕ in the range $0 \leq \theta \leq \pi$ and $0 \leq \phi \leq 2\pi$. Typical examples of the topology of these contour plots are displayed in Figures 2a-c for simulated shocks and Figures 5a-c for real shocks. These plots exhaustively illustrate the location in the polar shock normal angles (ϕ, θ) where the $\log\chi^2(\theta, \phi)$ is a minimum. The gradient search selected location will correspond to a possible solution of the problem. However, if more than one minimum is present, each must be studied independently to determine the (ϕ, θ) direction that is most consistent with the supplementary tests which characterizes a shock solution. If this situation occurs, additional information (as discussed in section 4) is required to ascertain the appropiate physical shock solution. Once the normal $\vec{n}$ is obtained, equation (13) and the data are used to determine the optimal shock speed V_s.

The solution for V_s can be presented also as a one dimensional least squares problem. However, because V_s enters linearly in equation (13), it can be shown that the least squares problem has an analytic solution for the shock speed. To show this we write the least squares objective function $\chi^2(V_s)$ that must be minimized

$$\chi^2(V_s) = \sum_{i=1}^{N} \left(\frac{\Delta[\rho_i \vec{V}_i]}{\Delta[\rho_i]} \cdot \vec{n} - V_s \right)^2 / \sigma^2$$

where the first term in parentheses corresponds to the shock velocity as determined from the observations and σ is the standard deviation of the shock speed obtained from the data. The value of $\vec{n}$ used in this calculation is the one obtained in the first part of this section. If we now take the

first and second derivative of $\chi^2(V_s)$ with respect to V_s it can be easily shown that the point V_s where the minimum occurs is given by

$$V_s = \frac{1}{N} \sum_{i=1}^{N} \frac{\Delta[\rho_i \vec{V}_i]}{\Delta[\rho_i]} \cdot \vec{n}$$

This is the only solution to the linear least squares problem in one dimension and its uniqueness can be analytically demonstrated by determining that the second derivative of $\chi^2(V_s)$ function is positive. The procedure in Appendix A gives similar results since both approaches are mathematically equivalent.

b. Determination of the Rankine-Hugoniot Constants

We now proceed to determine the RH conservation constants. For this calculation it is convenient to rewrite the equations (8) - (11) in terms of the conservation constants as follows:

$$G_n = \rho(\vec{V} \cdot \vec{n} - V_s) \tag{16}$$

$$B_n = \vec{B} \cdot \vec{n} \tag{17}$$

$$\vec{S}_t = \rho(\vec{V} - V_s\vec{n}) \cdot \vec{n} \; (\vec{V}\cdot(\underline{\underline{I}}-\vec{n}\vec{n})) - \frac{(\vec{B}\cdot\vec{n})}{4\pi} (\vec{B}\cdot(\underline{\underline{I}}-\vec{n}\vec{n})) \tag{18}$$

$$c\vec{E}_t = \vec{n} \times (\vec{V}\cdot(\underline{\underline{I}}-\vec{n}\vec{n})) \; (\vec{B} \cdot \vec{n}) - (\vec{V} \cdot \vec{n} - V_s) \; \vec{n} \times (\vec{B}\cdot(\underline{\underline{I}}-\vec{n}\vec{n})) \tag{19}$$

where the conservation constants G_n, B_n, $\vec{S}_t$ and $\vec{E}_t$ have been previously defined and c is the speed of light. An inspection of equations (16) - (19) indicates that these constants appear linearly and independently in the equations. This means that if we take the plasma and magnetic field in the right-hand side of equations (16) - (19) to be given by the measurements on

both sides of the shock, then the solution for the conservation constants reduces to a linear least squares problem whose solution can be obtained analytically. The method of obtaining these constants is similar to that previously used in the determination of the shock speed. Therefore the optimal conservation constants are given by

$$G_n = \frac{1}{2N} \sum_{i=1}^{2N} \rho_i \, (\vec{V}_i \cdot \vec{n} - V_s) \tag{20}$$

$$B_n = \frac{1}{2N} \sum_{i=1}^{2N} (\vec{B}_i \cdot \vec{n}) \tag{21}$$

$$\vec{S}_t = \frac{1}{2N} \sum_{i=1}^{2N} \left[\rho_i \, (\vec{V}_i \cdot \vec{n} - V_s) \, (\vec{V}_i \cdot (\underline{\underline{I}} - \vec{n}\vec{n})) - \frac{(\vec{B}_i \cdot \vec{n})}{4\pi} (\vec{B}_i \cdot (\underline{\underline{I}} - \vec{n}\vec{n})) \right] \tag{22}$$

$$c\vec{E}_t = \frac{1}{2N} \sum_{i=1}^{2N} [\vec{n} \times (\vec{V}_i \cdot (\underline{\underline{I}} - \vec{n}\vec{n}))(\vec{B}_i \cdot \vec{n}) - (\vec{V}_i \cdot \vec{n} - V_s) \, \vec{n} \times (\vec{B}_i \cdot (\underline{\underline{I}} - \vec{n}\vec{n}))] \tag{23}$$

These optimal solutions of the conservation constants are unique, corresponding to an absolute minimum of the objective χ^2 function, since they result from a linear least squares problem whose second derivative can be shown to be positive.

c. Determination of the self-consistent Rankine-Hugoniot asymptotic states

In this section we proceed to determine the compatible RH asymptotic states. This is the final problem in the least squares sequence presented. Substitution of equations (16) and (17) into the vector equations (18) and (19) yield a set of six equations in terms of the conservation constants, the shock normal and the shock speed. After some algebraic manipulations, these six equations can be solved together to obtain the vector expressions

$$\vec{V}(\rho) = \frac{G_n \vec{S}_t + \rho \frac{B_n}{4\pi} (\vec{n} \times c\vec{E}_t)}{G_n^2 - \rho B_n^2/(4\pi)} + \vec{n} \left(G_n/\rho + V_s \right) \tag{24}$$

$$\vec{B}(\rho) = \frac{\rho(B_n \vec{S}_t + G_n (\vec{n} \times c\vec{E}_t))}{G_n^2 - \rho B_n^2/(4\pi)} + \vec{n} B_n \tag{25}$$

An inspection of these equations indicates that both the velocity and the magnetic field are functions only of the unknown density since the shock normal, speed and conservation constants have been previously determined. This implies that we only need to solve for the density at each side of the shock to predict the compatible Rankine-Hugoniot states. Two other important conditions that resulted naturally from (24) - (25) by taking the dot product of these equations with the shock normal $\vec{n}$ are

$$\vec{n} \cdot \vec{S}_t = 0, \qquad \vec{n} \cdot \vec{E}_t = 0 \tag{26}$$

which means that in the frame of the observations, the product of the normal vector with the tangential momentum flux and electric field must vanish. This is not a surprising result since in the frame of the shock by definition these conditions must also be satisfied. These equations are singular for values of

$$\rho = 0, \qquad \rho = \frac{4\pi G_n^2}{B_n^2}$$

The first condition ($\rho = 0$) represents an unphysical solution since for the

existance of a shock the density at both sides must also exist. The second condition is more subtle and corresponds to solutions for which the asymptotic inflow speed is equal to the intermediate mode speed

$$M_A' = \left| \frac{\vec{V} \cdot \vec{n} - V_s}{\vec{V}_A \cdot \vec{n}} \right| = 1 \qquad (27)$$

Here we have defined $\vec{V}_A = \vec{B}/\sqrt{(4\pi\rho)}$ as the Alfvén velocity. This solution corresponds to a rotational discontinuity and not a shock. Notice that this is not inconsistent with the solution of the RH equations since a rotational discontinuity is also a solution to these equations. An inspection of the above equations shows that for any fast shock solution to exist the density must lie in the range $0 < \rho < 4\pi G_n^2/B_n^2$. In order for this regime to be physical requires that the mass flux G_n should be experimentally non-zero. For values of $\rho > 4\pi G_n^2/B_n^2$ the normal Alfvén Mach number (M_A') is less than unity and this could indicate that either the disturbance is a slow shock or is not a shock at all. To assess whether the solution corresponds to a slow shock, additional information such as the temperature of both electrons and ions of the plasma is required. Another important consequence of this condition is that for perpendicular shocks (i. e. $B_n = 0$) the singularity goes to infinity. This, of course, implies that only fast shock solution can exist in such conditions which is clearly compatible with MHD since slow shocks and rotational discontinuities becomes tangential discontinuities as θ_{Bn} approaches 90° [Landau and Lifshiftz, 1960].

To show the application of the least squares method to the system of equations (24) - (25) we again define a vector function $\vec{F}(\vec{x}; \vec{p})$ representing the six equations given by (24)-(25) and one additional equation given by

the density observations as follows:

$$\vec{F}(\vec{x}_i ; \vec{p}) = \begin{pmatrix} \vec{V}_i - \vec{V}(\rho) \\ \vec{B}_i - \vec{B}(\rho) \\ \rho_i - \rho \end{pmatrix} \tag{28}$$

The parameter $\vec{x}_i = (\rho, \vec{V}, \vec{B})_i$ represents the plasma and magnetic field observations at either the upstream or downstream sides of the shock. We also define the index i which varies from 1 to the number of data points N. The variable $\vec{p} = (\rho)$ represents the unknown parameter to be obtained. As in the case of the shock normal angles, the function $\vec{F}(\vec{x}_i ; \vec{p})$ can be expanded in Taylor series (as in equation (14)) about an initial guess density value $\vec{p}^{(o)} = (\rho^{(o)})$ to give the expression

$$\underline{\underline{A}}\ \Delta\vec{p} = \Delta\vec{Y} \tag{29}$$

which again represents the normal equation of least squares. In this case we define $\underline{\underline{A}}$ as a matrix of size N' × 1 (where N' = 7 × N) formed by the partial derivatives of the seven model equations representing velocity $\vec{V}$, magnetic field $\vec{B}$ and density ρ, evaluated at the initial guess. To avoid numerical errors, these derivatives have been calculated analytically and verified by a numerical quadrature. We also define $\Delta\vec{Y}$ as follows

$$\Delta\vec{Y} = \begin{pmatrix} \vec{V}_i - \vec{V}(\rho^{(o)}) \\ \vec{B}_i - \vec{B}(\rho^{(o)}) \\ \rho_i - \rho^{(o)} \end{pmatrix}$$

representing the difference between the observations and the model parameters.

The solution of the normal equation (29) is presented in Appendix A, however as in the shock normal angles situation, the final solution $\vec{p}^{*} = (\rho^{*})$ of (29) is obtained by an iterative scheme that minimizes the variance $\chi^2(\rho) = \vec{r}^{T}\,\vec{r}$ of the residuals. The determination of these asymptotic states can be divided in two parts. First, obtain by a least squares method the asymptotic state of the upstream side of the shock using the plasma and magnetic field observations, the previously determined shock normal, speed and the estimated conservation constants. By a similar procedure, the asymptotic states of the downstream side of the shock are determined. This approach is self-consistent since both sides of the shock yield the same conservation constants, shock normal and shock speed. To ascertain the 'uniqueness' of the non-linear least squares iterative solution we can simply graphically investigate the topology of the $\log\chi^2(\rho)$ function as a function of ρ at each side of the shock transition. In Figures 3a-c and Figures 6a-c we present examples of this function for simulated and real shocks, respectively. The solid and dashed lines represent the function $\log\chi^2(\hat{\rho})$ versus density $\hat{\rho}$ $(=\rho/\rho^{*})$ in the upstream and downstream sides, respectively. Because of the particular choice of the model equations (24)

- (25) which are singular for values of $\rho=0$ and $\rho = 4\pi G_n^2/B_n^2$, the $\chi^2(\rho)$ function has been pre-conditioned to discriminate against tangential, contact and rotational discontinuities. These RH solutions will correspond to the maximum of the $\chi^2(\rho)$ funtion for the singularity $\rho = 4\pi G_n^2/B_n^2$.

4. Applications And Comparisons With Other Methods

In this section we present the application and results of our method to both simulated and real shocks. We further compare the results obtained with those calculated by other techniques using the same data set. The simulated shocks were designed from the RH conservation equations [Tidman and Krall, 1971]. These shocks were constructed by prescribing the normal, the conservation constants, the shock speed and θ_{Bn} the angle between the shock normal and the upstream magnetic field. Once these parameters are specified the profiles of density, velocity and magnetic field were obtained. In an attempt to simulate the presence of waves or random noise in the data of an observed shock, the profiles of density, velocity and magnetic field were randomized independently. For simplicity, the random fluctuations superposed on these profiles were chosen to have a vanishing "time-average" with a relatively small amplitude ($\simeq$10%). The final profiles were then used to evaluate and recover the shock parameters. We have selected a perpendicular ($\theta_{Bn} = 90°$), parallel ($\theta_{Bn} = 0°$) and oblique ($\theta_{Bn} = 45°$) synthetic shock as samples to test the method. We have also estimated the shock parameters for two real interplanetary shocks seen by the Voyager 1 and 2 spacecrafts and a planetary bow shock crossing from the ISEE-1 spacecraft. Comparison of our results with other methods including the two spacecraft method for the bowshock crossing are also presented.

a. Synthetic Shocks

Figures 1a-c show plots of the magnitude and components of the magnetic field and the plasma bulk velocity, together with the plasma density in an

arbitrary cartesian coordinate system of a perpendicular, parallel and oblique simulated shocks respectively. These shocks are designed to have a θ_{Bn} = 90°, 0° and 45° respectively with a shock speed of 500 km/sec. The perpendicular shock profile satisfies the condition $\vec{B}/\rho$ = constant and $\vec{V}^*$ = constant/ρ where the density profile is arbitrarily chosen to be

$$\rho(t) = \rho_+ + \rho_- \tanh[(t-t_o)/\tau]$$

where $\rho_+ = (\rho_2 + \rho_1)/2$ and $\rho_- = (\rho_2 - \rho_1)/2$, τ controls the slope of the shock profile, t_o indicates the shock location and ρ_1, ρ_2 are the asymptotic densities. The parallel shock velocity profile was chosen to be $\vec{V}^*$ = constant/ρ and the magnetic field to be a constant across the transition zone. The density profile is chosen similar to the above expression for the perpendicular case. Although the synthetic shocks were constructed following Tidman and Krall [1971], we could have also designed them using equations (24) and (25) since they are equivalent. The oblique shock was designed following a new algorithm recently developed by Whang et al. [1985] which allow the construction of shocks for arbitrary θ_{Bn} angles (except 0° and 90°) given the plasma and magnetic field parameters in the upstream side.

The vertical lines in Figures 1a-c indicates the data interval selected at both sides of the transition to evaluate the shock parameters. We now draw attention to the fact that there is no specific procedure on how and where the data should be selected. The only known requirement is that the data selected should not contain information about the transition layer, because in this region the RH conservation equations are not valid. However, there is no clear prescription on how far away from this layer or

how much data can be used to determine the shock geometry. Nonetheless, once the data interval, representing an ensemble of possible upstream and downstream states, has been decided; there is no restriction in either selecting equal or unequal number of data points at each side of the transition layer. Alternatively, since our method converges rapidly, we can select various data intervals with different number of data points to obtain an ensemble of solutions of the shock geometry. Then, we can investigate the intersection of all the solutions, within their error bounds, to statistically assess the shock geometry.

The 'uniqueness' contour plot for the shock normal solution is presented for all the three cases in Figures 2a-c respectively. These figures show the contour levels of the logarithm of the χ^2 objective function formed from all the data selected at both sides of the shock and the RH conservation equations, versus all the possible shock normal polar angles θ and ϕ as described in section 3a. Also indicated are shaded regions corresponding to the lowest levels of the $\log\chi^2$ function, indicating the 95% confidence interval where the solution of the iterative scheme is located. Details about how to define such confidence intervals have been previously discussed by Scheffé [1959] and Bard [1974] and are presented in Appendix A. The topology of the 'uniqueness' surfaces of the perpendicular (Figure 2a) and the oblique shocks (Figure 2c) seems to be similar. Both surfaces show the solution to lie inside a "ridge" where the value of the contour levels are the smallest. However the topology of the parallel shock (Figure 2b) not only indicates the presence of a "ridge" but it shows a pair of "holes" at conjugate (i. e. anti-collinear) angles. It is important to note that the "holes" and "hills" shown in these topologies always appear in conjugate pairs due to the sign ambiguity in the shock normal solution. These

topologies seems to be typical of the type of shock in study, however this should be substantiated by a statistical study.

A search for a solution through all the holes shown in these figures indicates that not all of them correspond to the proper shock solution of the problem. To assess the proper shock-like solution, four conditions must be considered. First, we should certify a defensibly non-vanishing mass flux G_n (i. e. $|\delta G_n/G_n| < 1$). Secondly, we must compare the quality of the asymptotic magnetofluid states predicted with the corresponding observed variables and determine whether such predictions are within the standard deviations of the measurements. Thirdly, using the asymptotic magnetofluid variables we determine the Alfvén Mach number ($M_A = M_A' \cos\theta_{Bn}$). If the quality of the asymptotic states is acceptable and the diagnosis of the problem indicates a fast shock solution, then the normal Alfvén Mach number must be theoretically greater than unity. However, if the normal Alfvén Mach number is computationally smaller than unity, suggesting the possibility of a slow shock, we must consider the relative mass flux error $|\delta G_n/G_n|$ and the additional temperature information to correctly assess the final solution. Finally, using the RH equation (5) we may predict the thermal pressure jump across the shock given by

$$\Delta(\vec{n}\cdot\underline{\underline{P}}\cdot\vec{n}) = \Delta P = -\left[\left(\frac{B^2}{8\pi} + \rho(\vec{V}\cdot\vec{n}-V_s)^2\right)_d - \left(\frac{B^2}{8\pi} + \rho(\vec{V}\cdot\vec{n}-V_s)^2\right)_u\right]$$

where the subscripts "d" and "u" represent the downstream and upstream sides respectively. Note that the prediction of the scalar normal pressure jump across the shock is independent of an assumption of an equation of state. To evaluate ΔP we use the predicted asymptotic magnetofluid variables. If

ΔP yield a negative pressure value, then the "hole" selected cannot correspond to a shock.

The shock normal solution obtained by the pre-averaged and iterative schemes are also presented in Figures 2a-c. These solutions are indicated by various symbols corresponding to the method indicated in Tables 1a-c. In situations where different methods yield the same solution or very near each other, the symbol indicator corresponding to each technique will point with an arrow to the proper location in the contour plots to avoid overcrowding the solutions.

To determine either the θ_{Bn} angle defined by $\theta_{Bn} = \cos^{-1}(\vec{B}^u \cdot \vec{n}/|\vec{B}^u|)$, the Alfvén Mach number M_A ($= M_A' \cos\theta_{Bn}$), or the pressure jump condition, it is necessary to evaluate the asymptotic states. By evaluating the optimal density state at each side of the shock, the self consistent asymptotic velocity and magnetic field are 'uniquely' determined. Figures 3a-c show the 'uniqueness' of the solution for the evaluation of the asymptotic states in all three cases. These figures indicate the levels of the $\log\chi^2(\rho)$ objective function formed from the data selected at both sides of the shock and the model equation (28) versus the normalized density $\hat{\rho} = \rho/\rho^*$ as described in section 3c. In Figures 3a-c the solid and dashed curves represents the $\log\chi^2(\rho)$ for the upstream and downstream side of the transition layer, respectively. The normalization density ρ^* corresponds to the final predicted value determined by the iteration scheme at each side of the shock. For the three types of simulated shocks presented, these curves only contain a single minimum corresponding to the value correctly determined by the iteration scheme. The fact that only one minimum exists at a density value ρ^* in the range $0 < \rho < 4\pi G_n^2/B_n^2$ indicate, not only the 'uniqueness' of the shock-like solution for the density, but also for the

asymptotic velocity $\vec{V}(\rho^*)$ and magnetic field $\vec{B}(\rho^*)$ as described in equations (24) and (25). Note also that Figures 3a-c show the singular behavior of the $\chi^2(\rho)$ function when $\rho = 0$. We previously have established the existance of another singularity $\rho = 4\pi G_n^2/B_n^2$ in section 3c which indicates the transition from fast to slow shock. This singularity also exists in these cases, but they are located far away from the $\chi^2(\rho^*)$ minimum and off the figures.

The general results for the three synthetic shocks are summarized in Tables 1a-c. These tables contain the results obtained from the pre-averaged and iterative methods for the geometrical characteristics of the shocks. For comparison, the first column contains the exact solution of the shock geometry of the synthetic shocks and the last column indicated by VS shows the solution obtained by our method. The first nine rows show the geometrical parameters that describe the shock geometry. The next fourteen rows show the asymptotic magnetofluid variables used by the pre-average methods and those determined from the iterative schemes. Finally, the last two rows give a measure of the efficiency of the iterative schemes in obtaining a solution.

For the perpendicular shock (Figure 2a) the solution of our iterative scheme gives a $\theta_{Bn} = 90.0° \pm 2°$ and a shock speed of about 503 ± 17 km/sec. The final solution is located at $\theta = 20° \pm 0.1°$ and $\phi = 160° \pm 14.7°$ as indicated by the dark circle inside the shaded region (95% confidence interval) along a ridge in Figure 2a. At this location the final value of the $\log\chi^2$ is -0.33. The path followed by the descending iterative gradient scheme has been indicated by the connected circles. Because of the sign ambiguity in the shock normal, a second solution exists at conjugate angles $\theta = 160° \pm 0.1°$ and $\phi = 340° \pm 14.7°$. This second solution represents the

normal vector opposite (anti-collinear) to the one indicated in Table 1a and has a V_s of opposite sign to its mirror image. Both solutions are perfectly valid, however in general the proper sign of the solution is decided by compensating the sign of the scalar shock speed V_s with the obtained normal to form the vector shock velocity $\vec{V}_s = V_s\vec{n}$. Besides our solution we also show in Figure 2a the solution obtained by other methods. The general results of the analysis for this perpendicular shock are presented in Table 1a. A comparison with other methods of the results suggests that except for the LA method whose convergence to a solution was extremely slow and for the MC method, which did not reproduce the known solution accurately enough, all other procedures yield reasonable results relative to the exact solution. The reason the MC method gave a poor solution seems to be related to the fact that the MC equation

$$\vec{n} = \pm \frac{(\vec{B}_1\times\vec{B}_2)\times(\vec{B}_1-\vec{B}_2)}{|(\vec{B}_1\times\vec{B}_2)\times(\vec{B}_1-\vec{B}_2)|}$$

becomes singular for perpendicular shocks. The convergence in the LA method was too slow because at each step in the iteration process it depends on the same expression of magnetic coplanarity (MC) [Lepping and Argentiero, 1971]. Besides, we noticed that the LA method is allowed to search for solutions in unphysical regions where, for example, the density is predicted negative. In consequence, this kind of unconstrained scheme slows down the iteration process and permits the gradient search to take large steps that may well violate the initial local Taylor series expansion. Recently Acuna and Lepping [1984] attempted to speed up the convergence rate of the LA method. Although some increase in the rate of convergence was obtained, this has not controlled and constrained the search in unphysical regimes. One important

aspect which arises from the results in Table 1a is that both the AS method given by

$$\vec{n} = \pm \frac{[(\vec{B}_2-\vec{B}_1)\times(\vec{V}_2-\vec{V}_1)]\times(\vec{B}_1-\vec{B}_2)}{|[(\vec{B}_2-\vec{B}_1)\times(\vec{V}_2-\vec{V}_1)]\times(\vec{B}_1-\vec{B}_2)|}$$

and the VC method given by

$$\vec{n} = \pm \frac{(\vec{V}_2-\vec{V}_1)}{|(\vec{V}_2-\vec{V}_1)|}$$

yield accurate solutions for the perpendicular shock geometry. Although the VC method is an approximate technique, in the case of high Mach number perpendicular shocks, it is theoretically expected to produce the proper solution as argued by Abraham-Shrauner and Yun [1976].

Another aspect which resulted from the analysis of the contours in Figure 2a is the existence of two unphysical minima located at conjugate pair of angles $\theta = 90° \pm 10°$ and $\phi = 70°$ and $250° \pm 10°$. This class of minima are almost always present in the contours. Their location are nearly orthogonal to the proper optimal solution. These solutions yields $M_A' < 1$ and the magnetofluid variables determined from them are in very poor agreement with the plasma and magnetic field observations. Moreover, these solutions violate the pressure jump condition across the shock layer. An inspection of these unphysical shock solutions suggests that they seem to belong to either the family of the tangential, contact or rotational discontinuities since the mass flux is numerically extremely small.

A similar analysis has been performed for a synthetic parallel shock as shown in Figure 1b. The plots in Figures 2b and 3b show the 'uniqueness' of

the shock normal solution and the magnetofluid variables for this shock. Superposed on Figure 2b we show the locus of the descending path of the iterative scheme and the solutions by other methods. The general results of the analysis of these shocks are tabulated in Table 1b. The results of our iterative scheme yield $\theta_{Bn} = 0.03° \pm 5°$ with a shock speed of 500 ± 12 km/sec. The final solution of the parallel shock is indicated by the dark circle in Figure 2b at the polar angles $\theta = 20° \pm 11.8°$ and $\phi = 160° \pm 34.6°$ located in one of the isolated shaded "holes". At this location the final value of $\log\chi^2$ is 1.28. Similarly there is a conjugate solution at $\theta = 160.1° \pm 11.8°$ and $\phi = 340° \pm 34.6°$ corresponding to the opposite sign of the shock normal. Both solutions are physical since they predict a positive pressure jump across the layer. For this case the LA method did not converge within a reasonable time. Furthermore, neither the MC method nor the AS method predicted the correct solution for this shock because of the singular behavior that both methods have as the θ_{Bn} approaches 0°. The location of the MC and AS solutions, shown in Figure 2b, indicates that they reside in a deep shaded 'ridge', where the χ^2 function is small and where the unphysical solution exists. On the other hand the VC method gave good results that lies within the 95% confidence level of the minimum. However this agreement may be fortuitous because in the design of the parallel shock, the normal was chosen to be along the direction of the flow velocity which is a basic assumption of the VC method.

The analysis of the oblique shock in Figure 1c yield a solution of $\theta_{Bn} = 45.2° \pm 8°$ and a shock speed of 499.8 ± 19 km/sec. This final solution is indicated in Figure 2c by the dark circle along the shaded "ridge" at the polar angles $\theta = 20.8° \pm 1.0°$ and $\phi = 159.3° \pm 46.0°$. A conjugate solution is also present at $\theta = 159.2° \pm 1°$ and $\phi = 339.3° \pm 46.0°$. The results of

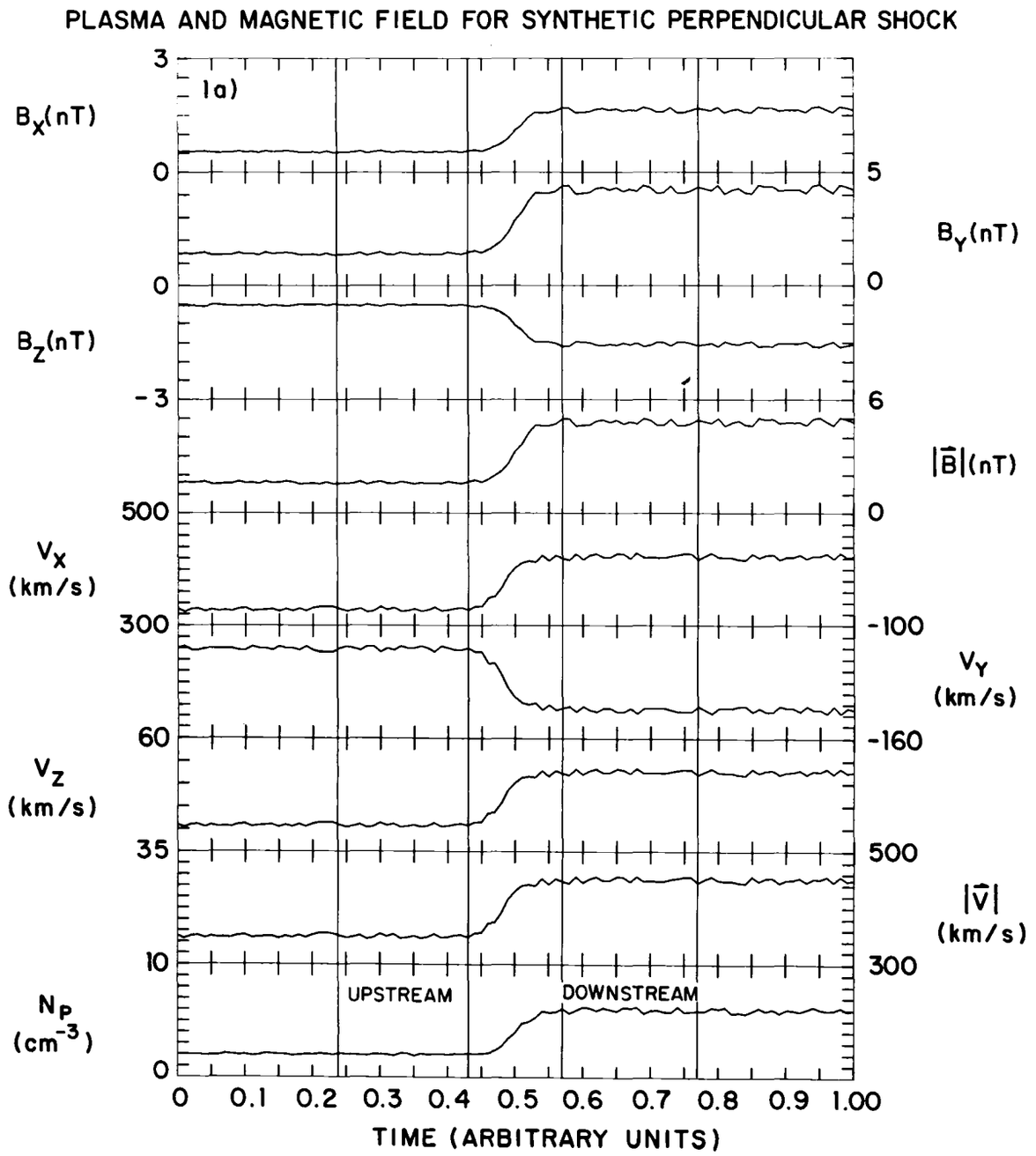

Figure 1a. Magnetic field and plasma data plots of a synthetic perpendicular shock. Vertical lines indicates the data interval selected for the shock geometry analysis at both sides of the layer. The horizontal axis represents time in arbitrary units and the shock time is 0.5.

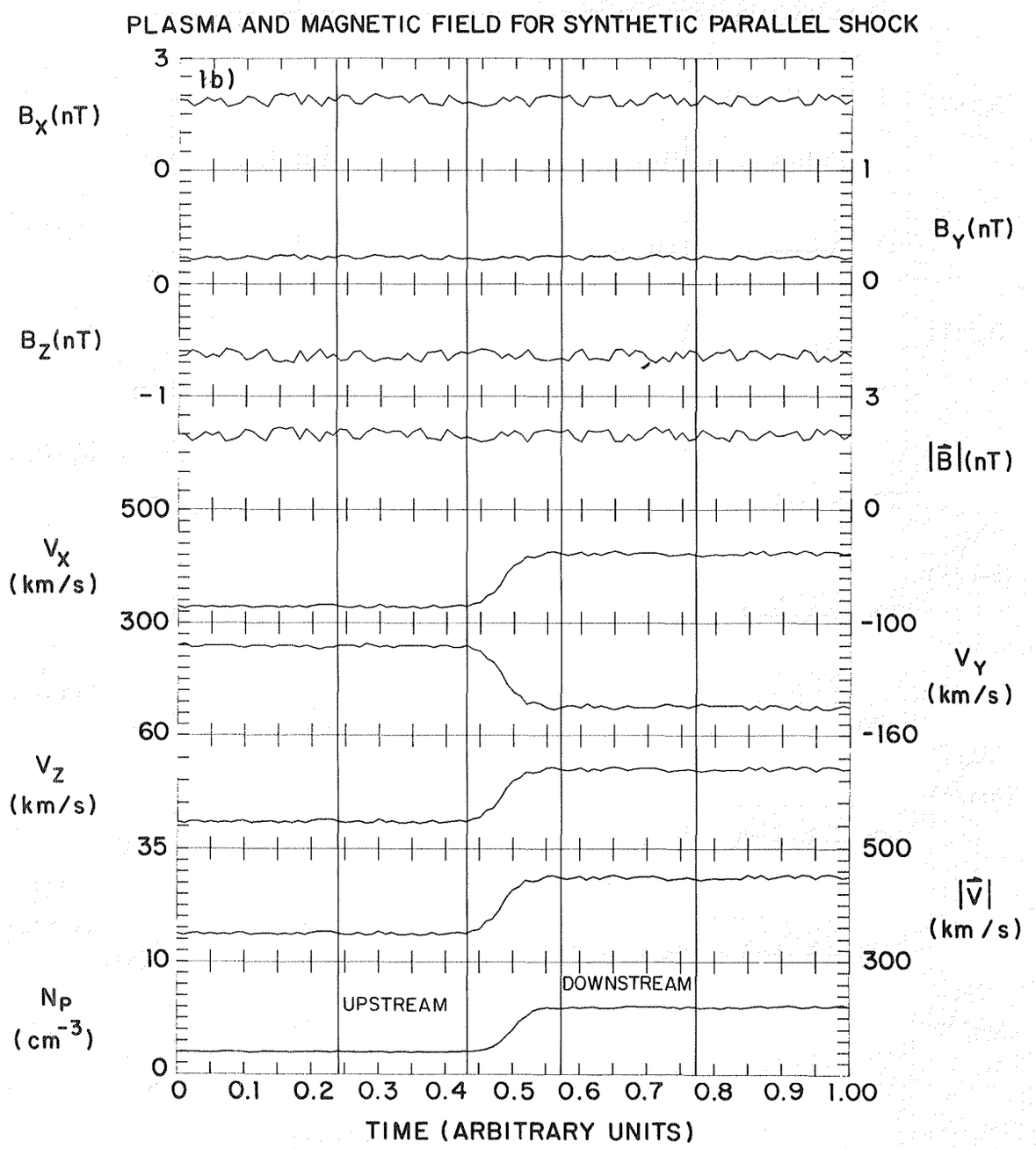

Figure 1b. Magnetic field and plasma data plots of a synthetic parallel shock. Vertical lines indicates the data interval selected for the shock geometry analysis at both sides of the layer. The horizontal axis represents time in arbitrary units and the shock time is 0.5.

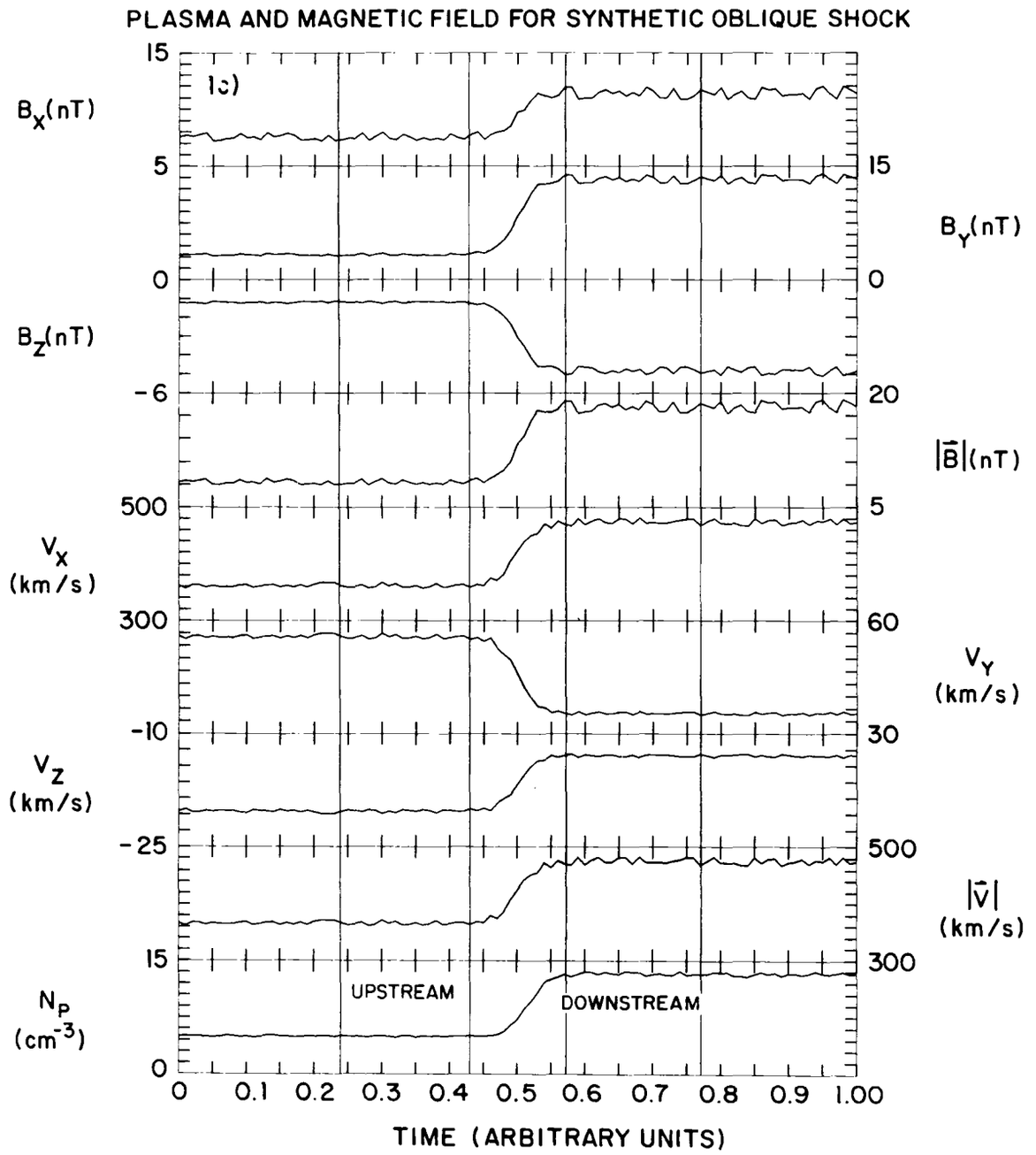

Figure 1c. Magnetic field and plasma data plots of a synthetic oblique shock. Vertical lines indicates the data interval selected for the shock geometry analysis at both sides of the layer. The horizontal axis represents time in arbitrary units and the shock time is 0.5.

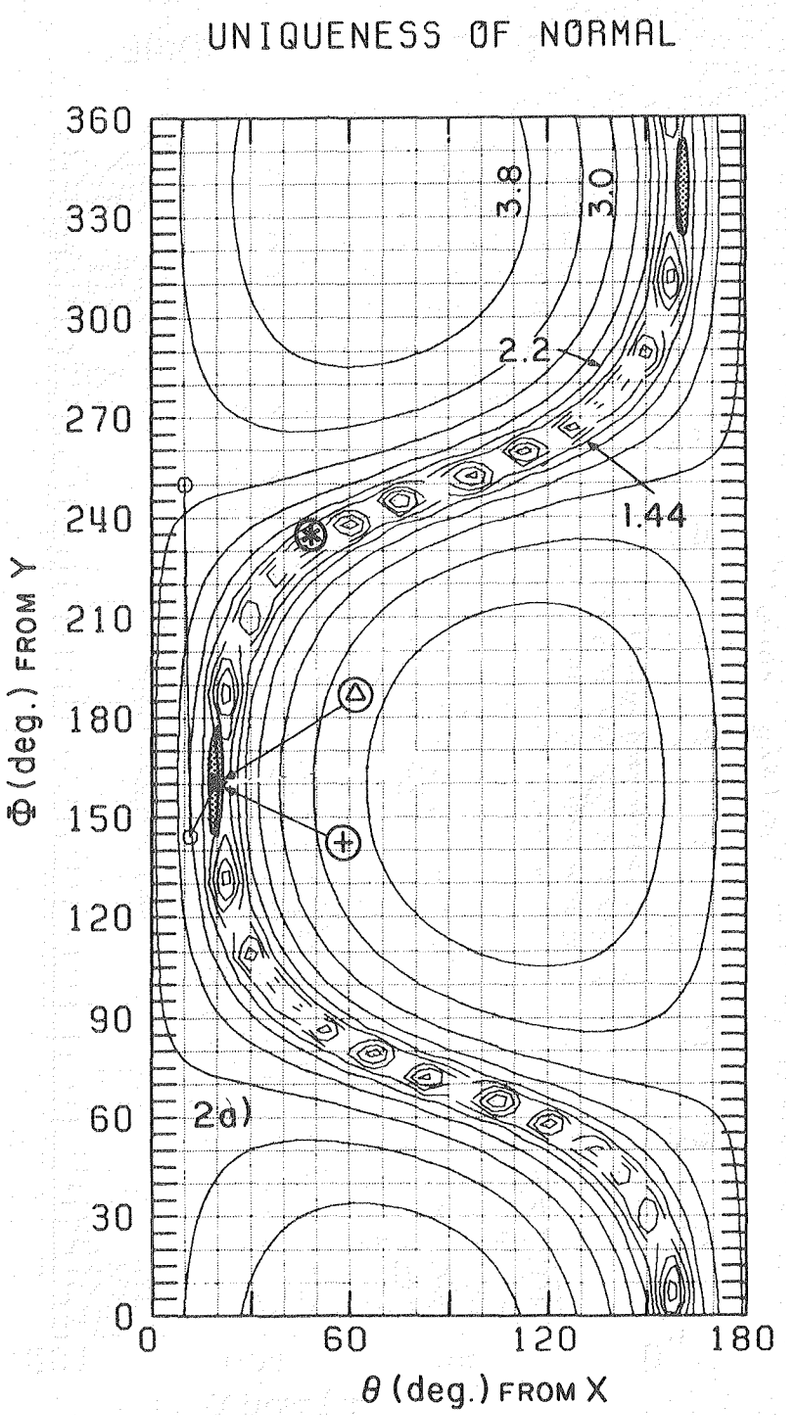

Figure 2a. Contour plots of the log χ^2 (θ, ϕ) function versus the shock normal polar angles (θ, ϕ) indicating the 'uniqueness' of the shock geometry for a synthetic perpendicular shock. Superimposed on these figures we indicate the location of the solution by magnetic coplanarity (MC) '*', velocity coplanarity (VC) '+', Abraham-Shrauner (AS) 'Δ', Lepping-Argentiero (LA) '□' and our solution (VS) '●'.

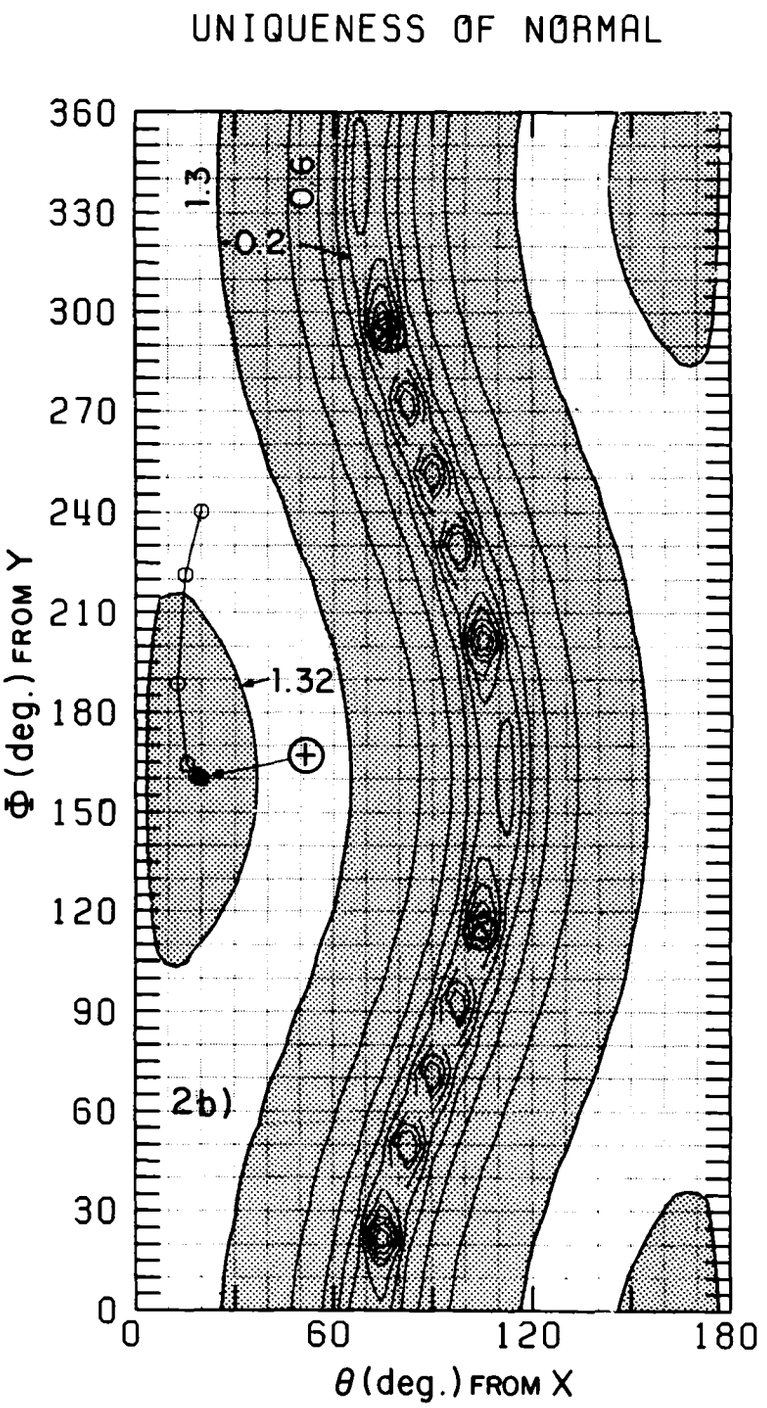

Figure 2b. Contour plots of the log χ^2 (θ, ϕ) function versus the shock normal polar angles (θ, ϕ) indicating the 'uniqueness' of the shock geometry for a synthetic parallel shock. Superimposed on these figures we indicate the location of the solution by magnetic coplanarity (MC) '*', velocity coplanarity (VC) '+', Abraham-Shrauner (AS) 'Δ', Lepping-Argentiero (LA) '□' and our solution (VS) '●'.

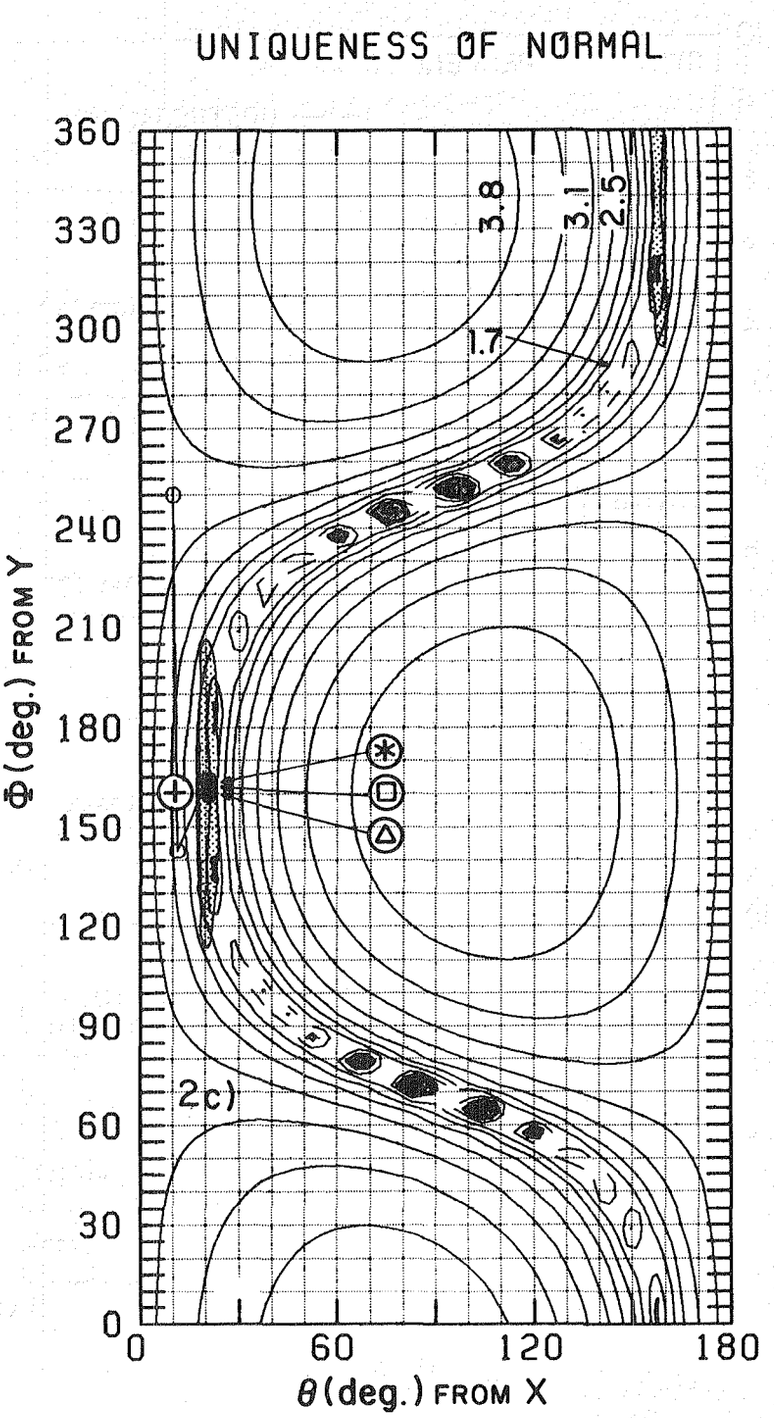

Figure 2c. Contour plots of the log χ^2 (θ, ϕ) function versus the shock normal polar angles (θ, ϕ) indicating the 'uniqueness' of the shock geometry for a synthetic oblique shock. Superimposed on these figures we indicate the location of the solution by a magnetic coplanarity (MC) '*', velocity coplanarity (VC) '+', Abraham-Shrauner (AS) 'Δ', Lepping-Argentiero (LA) '□' and our solution (VS) '●'.

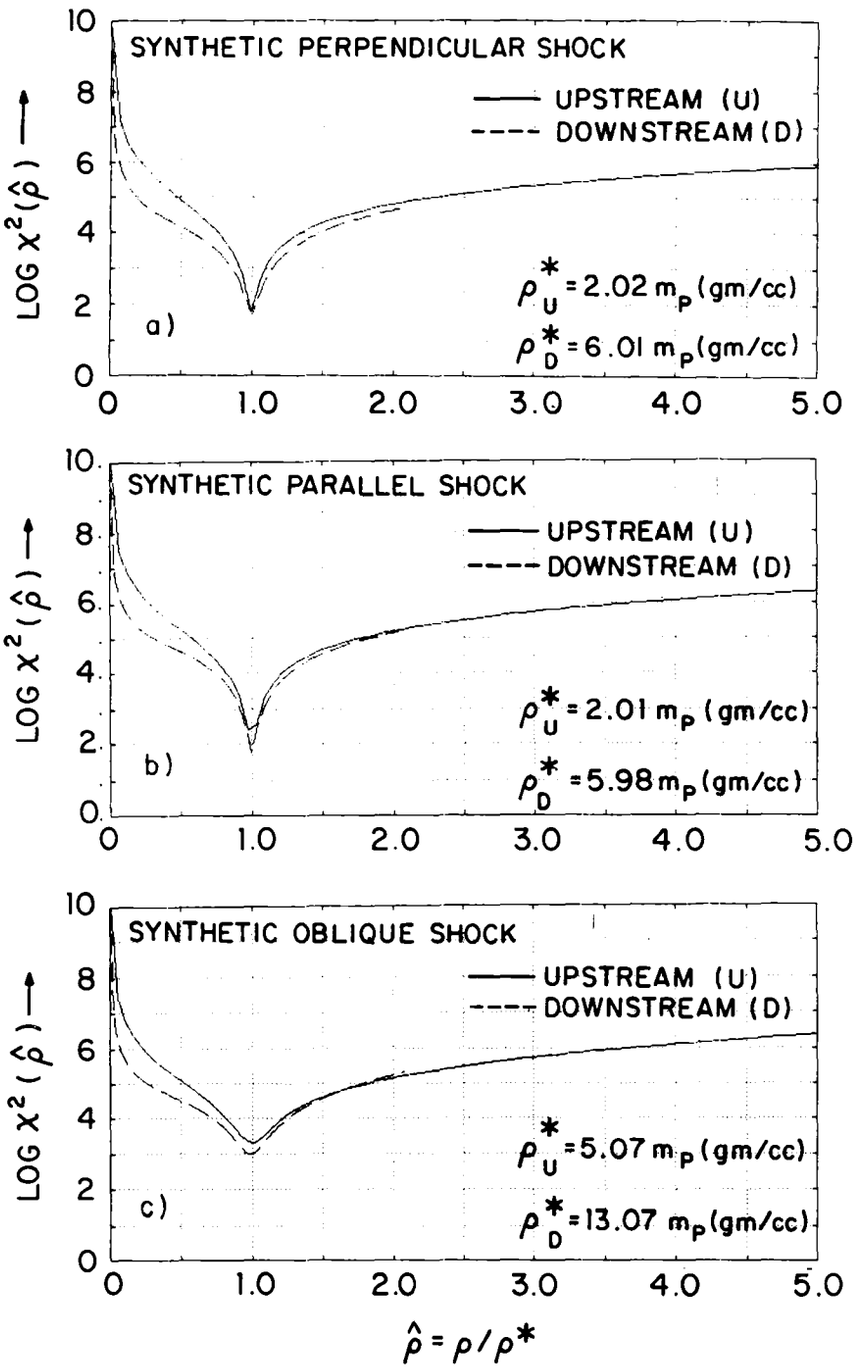

Figure 3. Plots of the log χ^2 $(\hat{\rho})$ function versus the normalized density $\hat{\rho} = \rho/\rho^*$ indicating the 'uniqueness' of the asymptotic magnetofluid variables in the upstream and downstream sides of a synthetic (a) perpendicular, (b) parallel and (c) oblique shocks. The normalization constant ρ^* is the value obtained by the iteration scheme at the minimum of the χ^2 function for each side of the shock.

Table 1a. Results of the analysis of the synthetic perpendicular shock.

		PRE-AVERAGED METHODS			ITERATIVE SCHEMES	
	Exact Solution	Magnetic Coplanarity MC(°)	Velocity Coplanarity VC(◇)	Abraham-Shrauner AS(△)	Lepping-Argentiero LA(□)	Vinas-Scudder VS(○)
θ_{Bn}(deg)	90.0	90.0	90.0	90.0	-	90.0
V_s(Km/s)	500.0	351.2	502.6	502.6	-	502.7
δV_s(Km/s)	-	-	-	-	-	±17.1
$\hat{n}_x$	0.9397	0.6566	0.9397	0.9397	-	0.9397
$\hat{n}_y$	-0.3214	-0.4693	-0.3214	-0.3214	-	-0.3214
$\hat{n}_z$	0.1170	-0.5905	0.1170	0.1170	-	0.1170
$\delta\Omega_n$(deg)	-	-	-	-	-	±2.1
M_A	6.1	4.4	6.3	6.3	-	6.3
ΔP(ev/cc)	262.2	110.9	279.8	279.8	-	281.3
n_1(part/cc)	2.00	2.02	2.02	2.02	-	2.02
V_{x1}(Km/s)	328.9	327.9	327.9	327.9	-	327.7
V_{y1}(Km/s)	-112.5	-112.1	-112.1	-112.1	-	-112.1
V_{z1}(Km/s)	40.9	40.8	40.8	40.8	-	40.8
B_{x1}(nT)	0.55	0.54	0.54	0.54	-	0.55
B_{y1}(nT)	1.41	1.40	1.40	1.40	-	1.41
B_{z1}(nT)	-0.51	-0.51	-0.51	-0.51	-	-0.51
n_2(part/cc)	6.0	6.0	6.0	6.0	-	6.01
V_{x2}(Km/s)	422.9	423.7	423.7	423.7	-	423.8
V_{y2}(Km/s)	-144.6	-144.9	-144.9	-144.9	-	-145.0
V_{z2}(Km/s)	52.6	52.7	52.7	52.7	-	52.8
B_{x2}(nT)	1.64	1.63	1.63	1.63	-	1.63
B_{y2}(nT)	4.24	4.21	4.21	4.21	-	4.20
B_{z2}(nT)	-1.54	-1.53	-1.53	-1.53	-	-1.53
No. iter	-	-	-	-	$>10^4$	5
T_c (sec)	-	-	-	-	$>10^4$	413.6

Table 1b. Results of the analysis of the synthetic parallel shock.

		PRE-AVERAGED METHODS			ITERATIVE SCHEMES	
	Exact Solution	Magnetic Coplanarity MC(*)	Velocity Coplanarity VC(+)	Abraham-Shrauner AS(Δ)	Lepping-Argentiero LA(□)	Vinas-Scudder VS(●)
θ_{Bn}(deg)	0.0	89.9	0.0	89.9	-	0.03
V_s(Km/s)	500.0	1.33	501.6	-1.3	-	500.1
δV_s(Km/s)	-	-	-	-	-	±11.7
$\hat{n}_x$	0.9397	-0.2395	0.9397	0.2396	-	0.9400
$\hat{n}_y$	-0.3214	-0.3840	-0.3214	0.3844	-	-0.3207
$\hat{n}_z$	0.1170	0.8917	0.1170	-0.8915	-	0.1166
$\delta\Omega_n$(deg)	-	-	-	-	-	±28.5
M_A	4.87	0.01	5.02	0.01	-	4.89
ΔP(ev/cc)	313.3	-0.1	323.1	-0.1	-	316.5
n_1(part/cc)	2.00	2.01	2.01	2.01	-	2.01
V_{x1}(Km/s)	328.9	328.3	328.3	328.3	-	328.3
V_{y1}(Km/s)	-112.5	-112.3	-112.3	-112.3	-	-112.3
V_{z1}(Km/s)	40.9	40.9	40.9	40.9	-	40.9
B_{x1}(nT)	1.88	1.89	1.89	1.89	-	1.88
B_{y1}(nT)	-0.64	-0.65	-0.65	-0.65	-	-0.64
B_{z1}(nT)	0.23	0.24	0.24	0.24	-	0.23
n_2(part/cc)	6.00	5.98	5.98	5.98	-	5.98
V_{x2}(Km/s)	422.9	422.3	422.3	422.3	-	422.3
V_{y2}(Km/s)	-144.6	-144.4	-144.4	-144.4	-	-144.4
V_{z2}(Km/s)	52.6	52.6	52.6	52.6	-	52.6
B_{x2}(nT)	1.88	1.87	1.87	1.87	-	1.88
B_{y2}(nT)	-0.64	-0.64	-0.64	-0.64	-	-0.65
B_{z2}(nT)	0.23	0.23	0.23	0.23	-	0.24
No. iter	-	-	-	-	$>10^3$	8
T_c (sec)	-	-	-	-	$>10^4$	338.0

Table 1c. Results of the analysis of the synthetic oblique shock.

		PRE-AVERAGED METHODS			ITERATIVE SCHEMES	
	Exact Solution	Magnetic Coplanarity MC(⊕)	Velocity Coplanarity VC(+)	Abraham-Shrauner AS(△)	Lepping-Argentiero LA(□)	Vinas-Scudder VS(⊕)
θ_{Bn}(deg)	45.0	45.1	35.8	45.1	44.5	45.2
V_s(Km/s)	500.0	502.3	529.8	502.3	536.2	499.8
δV_s(Km/s)	-	-	-	-	-	±18.6
$\hat{n}_x$	0.9397	0.9392	0.9826	0.9392	0.9418	0.9352
$\hat{n}_y$	-0.3214	-0.3226	-0.1744	-0.3226	-0.3226	-0.3318
$\hat{n}_z$	0.1170	0.1174	0.0635	0.1174	0.0947	0.1251
$\delta\Omega_n$(deg)	-	-	-	-	-	±8.5
M_A	2.2	2.3	2.3	2.3	-	2.3
ΔP(ev/cc)	404.0	456.2	486.2	456.2	875.1	374.6
n_1(part/cc)	5.00	5.02	5.02	5.02	5.06	5.07
V_{x1}(Km/s)	362.4	361.1	361.1	361.1	-	372.2
V_{y1}(Km/s)	55.9	55.6	55.6	55.6	-	78.8
V_{z1}(Km/s)	-20.3	-20.3	-20.3	-20.3	-	-28.9
B_{x1}(nT)	7.55	7.50	7.50	7.50	7.47	7.36
B_{y1}(nT)	3.31	3.29	3.29	3.29	3.24	3.14
B_{z1}(nT)	-1.20	-1.20	-1.20	-1.20	-1.23	-1.14
n_2(part/cc)	13.30	13.28	13.28	13.28	13.23	13.07
V_{x2}(Km/s)	473.8	474.7	474.7	474.7	-	463.7
V_{y2}(Km/s)	35.4	35.5	35.5	35.5	-	11.1
V_{z2}(Km/s)	-12.9	-12.9	-12.9	-12.9	-	-3.7
B_{x2}(nT)	11.41	11.35	11.35	11.35	11.29	11.58
B_{y2}(nT)	13.29	13.21	13.21	13.21	13.36	13.60
B_{z2}(nT)	-4.84	-4.81	-4.81	-4.81	-4.76	-4.98
No. iter	-	-	-	-	30	10
T_c (sec)	-	-	-	-	$>10^4$	386.3

the analysis for this shock are summarized in Table 1c. From the results in Table 1c we note that the MC and AS methods yield reasonable solutions, however the VC solution resulted in poor agreement with the exact solution. This is due to the mis-alignment of the bulk velocity to the shock normal and also probably to the small value of the Alfvén Mach number. The angle θ_{Bn} and the shock speed V_s given by the VC method are well outside the confidence bounds of the proper minimum solution. On the other hand, the LA method yielded good θ_{Bn} angle within the 95% confidence region; however, both the LA shock speed and pressure jump across the shock depart considerably from the exact solution. Note that the LA method cannot predict the asymptotic plasma bulk velocity at each side of the shock, but it can only resolve the velocity jump $\Delta\vec{V} = \vec{V}_2 - \vec{V}_1$ across the layer. The predicted velocity jump across the layer obtained by the LA method for this case yielded $\Delta\vec{V}$ = (115.8, -68.9, 21.6) km/sec which compares relatively well with the exact velocity jump $\Delta\vec{V}$ = (111.4, -20.5, 7.4) km/sec obtained from Table 1c. Moreover, we find a conjugate pair of unphysical solutions at θ = 90° ± 5° and ϕ = 70° and 250° ± 5° that violate the pressure jump condition across the shock and are located almost orthogonal to the proper solution. This unphysical "holes" also give a very small mass flux suggesting that this candidate solution is either a tangential or a contact discontinuity.

b. Real Interplanetary and Planetary Shocks

Complete plots of the magnitude and components of the magnetic field and plasma bulk velocity, with the plasma density in a heliocentric (R, T, N) coordinate system for a quasi-perpendicular and a quasi-parallel interplanetary shock are presented in Figures 4a-b, respectively. A similar plot for a planetary quasi-perpendicular bow shock in a GSE (geocentric

solar ecliptic) coordinate system is also shown in Figure 4c. The intervals selected for the analysis of the shock geometry are indicated by the vertical lines.

The event on November 27, 1977 corresponds to a quasi-perpendicular forward shock at 2225:57 UT as seen by the Voyager 1 at about 1.6 AU. Figures 5a and 6a represents the 'uniqueness' plots for the shock normal and asymptotic magnetofluid variables solutions respectively. Superposed on Figure 5a are the solutions obtained by other techniques. The path followed by the iterative gradient scheme to get to our solution is indicated by the connected circles. The results of this event are tabulated in Table 2a. First, note the similarity of the topology of the shock normal conjugate pair of solutions to that of the simulated perpendicular shock. As before, the solutions are along a "ridge" path and are located at two "thin" shaded contours centered about $\theta = 37.5° \pm 1.8°$ and $\phi = 262.5° \pm 22°$ and $\theta = 142.5° \pm 1.8°$ and $\phi = 82.5° \pm 22°$ where the value of $\log\chi^2$ is -0.014. Our estimates confirm that this event is a quasi-perpendicular shock with a $\theta_{Bn} = 84.2° \pm 9°$ and a shock speed of 305.5 ± 19 km/sec. Comparison of our solution with those obtained by other methods is shown in Table 2a. An inspection of the asymptotic magnetofluid variables predicted by our method, compared to the average values used by the pre-averaged techniques, and their standard deviations as shown in the first column, indicates the good agreement of our predictions within the error bounds of the data. For this event the LA solution is unknown beacuse the method did not converge within a reasonable time. Nonetheless, both the AS and the VC methods yielded good solutions because the shock meets the preconditions of these methods. Both solutions lie within the 95% confidence region about the minimum and they are within the error bounds supported by the data and the calculations.

However, although the MC solution is not extremely different from those obtained by other methods, it is nevertheless, outside the accepted confidence level. We have also estimated for this event using the electron and proton data, the observed thermal scalar pressure jump across the shock layer. The average electron temperature in the upstream and downstream sides of the shock are 6.0 ev and 11.0 ev respectively. Similarly, the proton temperatures in the upstream and downstream sides are 0.8 ev and 3.5 ev, respectively. Assuming charge neutrality we find that the thermal pressure jump is about 224 ev/cc. The value predicted by our method (see Table 2a) gives 296 ev/cc. This discrepancy of about 30% in the prediction of $\Delta(\vec{n}\cdot\underline{\underline{P}}\cdot\vec{n})$ can be explained by taking into consideration the geometry and orientation of the electron detector in the Voyager 1 spacecraft. The fact that there is only one electron detector which points always perpendicular to the radial direction almost in the equatorial plane (i. e. T-N plane) certainly indicates that the temperature reported are underestimated since there is not enough directional coverage of the electron distribution function to determine the proper pressure tensor. Besides, the important temperature component required for the pressure jump calculation should be that along the normal. But since this event is a quasi-perpendicular shock, this indicates that we must evaluate $T_{\perp}$ with certainty. An inspection of the electron detector orientation seems to indicate that the temperature obtained from it is the parallel component because of the field geometry relative to the detector during this period.

The case on January 29, 1978 is a quasi-parallel reverse shock at 0918:39 UT seen by Voyager 2 at about 2 AU. This shock has been previously studied in association with its structure by Scudder et al. [1984] and in the context of upstream waves by Viñas et al. [1984]. The 'uniqueness"

plots for the shock normal and magnetofluid variables solutions resulting from our calculations are shown in Figures 5b and 6b respectively. The results by our technique and by the other methods are shown in Table 2b. For reference, the shock normal results of other methods are superposed in Figure 5b. We find and confirm that this event is a quasi-parallel shock with a $\theta_{Bn} = 29° \pm 18.0°$ and a speed of 261 ± 39 km/sec. The shock normal corresponding to this event is located at $\theta = 157.7° \pm 14.1°$ and $\phi = 125.9° \pm 31.1°$ with its conjugate normal at $\theta = 22.3° \pm 14.1°$ and $\phi = 305.9° \pm 31.1°$ where the value of the minimum $\log\chi^2$ is -0.9. Besides our solution, the AS method gives the only other result which lies within the error bounds of the accepted solution. All the other methods lie outside the 95% confidence interval. Note that the MC and LA methods are well outside the region where the minimum is located indicating that their solution are poorly resolved. Another important aspect of our calculations is the good agreement of the predicted thermal scalar pressure jump across the layer with the observed thermal pressure jump as obtained from the electron and proton data. The average electron temperature in the upstream and downstream sides of the shock are 6.1 ev and 6.2 ev respectively. The mean proton temperature in the upstream and downstream sides are 1.92 ev and 5.0 ev respectively. Assuming equal density for electrons and ions (quasineutrality) we find that the thermal pressure jump is about 6.4 ev/cc. Comparing this value with our prediction in Table 2b we find agreement well within the 10% error of the observed jump while that obtained by other methods are larger.

The final event we investigated is a planetary bow shock crossing from ISEE-1 spacecraft on November 7, 1977. The shock crossing time is at 2251:19 UT and the data intervals selected at each side of the layer for the

analysis are indicated by the vertical lines in Figure 4c. So far, we have used only proton plasma data to analyze the shock geometry. However, for this event we shall use the electron plasma data obtained from the Goddard three dimensional electron spectrometer. The 'uniqueness' plots for the shock normal and the asymptotic magnetofluid variables are shown in Figures 5c and 6c respectively. As usual, the locus of the iterative scheme and the results from all the methods are indicated in Figure 5c. The overall results of the analysis of this event are presented in Table 2c. Our analysis indicates that this event is a quasi-perpendicular shock with θ_{Bn} = 74.4° ± 20° with a shock speed of -8.4 ± 31 km/s. The solution is located inside one of the shaded "holes" representing the 95% confidence region at the polar angles θ = 164.9° ± 7.5° and ϕ = 332.9° ± 28° where the minimum of the $\log\chi^2$ is 1.7. Another conjugate solution is also found at θ = 15.1° ± 7.5° and ϕ = 152.9° ± 28° corresponding to the opposite normal sign selected in Table 2c. The solutions obtained by the AS and the VC methods are also very near the optimal minimum solution. Despite the fact that the AS and VC solutions are within the 95% confidence region, their relative shock speed error is greater than 10% compared to the shock speed determined from the two spacecraft method. However, the MC and LA methods yield very poor solutions, which are well outside the acceptable confidence interval. Indeed, the MC solution is quite close to one of the unphysical solutions of the problem. For comparison, the velocity jump across the shock determined by the LA method gives $\Delta\vec{V}$ = (15.4, -56.3, 56.2) km/sec while our solution (VS) gives $\Delta\vec{V}$ = (197.2, -46.0, 26.5) km/sec. Figure 5c also show the presence of a conjugate pair of unphysical shock solutions that yield negative pressure jump across the shock layer. These unphysical shock 'solutions' are located at θ = 76° ± 8° and ϕ = 353° ± 9.5° and also at its

conjugate position $\theta = 104° \pm 8°$ and $\phi = 173° \pm 9.5°$. This bow shock has been exhaustively investigated by Scudder et al. [1985]. They have reported two spacecraft calculations of the shock speed using the ISEE-1 and -2 observations of the same shock crossing. We have compared our calculations of the shock speed with that determined by the two spacecraft time delay method and the result is in excellent agreement with it. From the separation distance between the spacecrafts $\Delta\vec{S}$ = (115.2, -193.0, 111.4) km, the time delay of the bow shock crossing Δt = 26 sec and assuming the shock normal determined by our method we can find the shock speed as seen by an observer in the spacecraft frame

$$V_s^{(spc)} = \frac{\Delta\vec{S} \cdot \vec{n}}{\Delta t}$$

Therefore the shock speed $V_s^{(spc)}$ gives -8.8 km/sec. A comparison with our results indicates an excellent agreement within the error bounds of the calculations. Scudder et al. [1985] have also reported the velocity using a somewhat larger data interval in the downstream side of the shock. Their solution is also consistent within their error bounds with that determined in this paper.

We have also evaluated and compared the thermal pressure jump $\Delta(\vec{n} \cdot \underline{\underline{P}} \cdot \vec{n})$ across the shock with that calculated from the electron and proton temperature data for the data interval indicated in Figure 4c. The average electron temperature in the upstream and downstream sides of the shock are 1.39 ev and 4.0 ev, respectively. Similarly, the proton temperatures in the upstream and downstream sides are 6.0 ev and 148.2 ev respectively. Assuming again charge neutrality we find that the observed thermal pressure jump across the shock is 4736.1 ev/cc. The predicted pressure jump (see

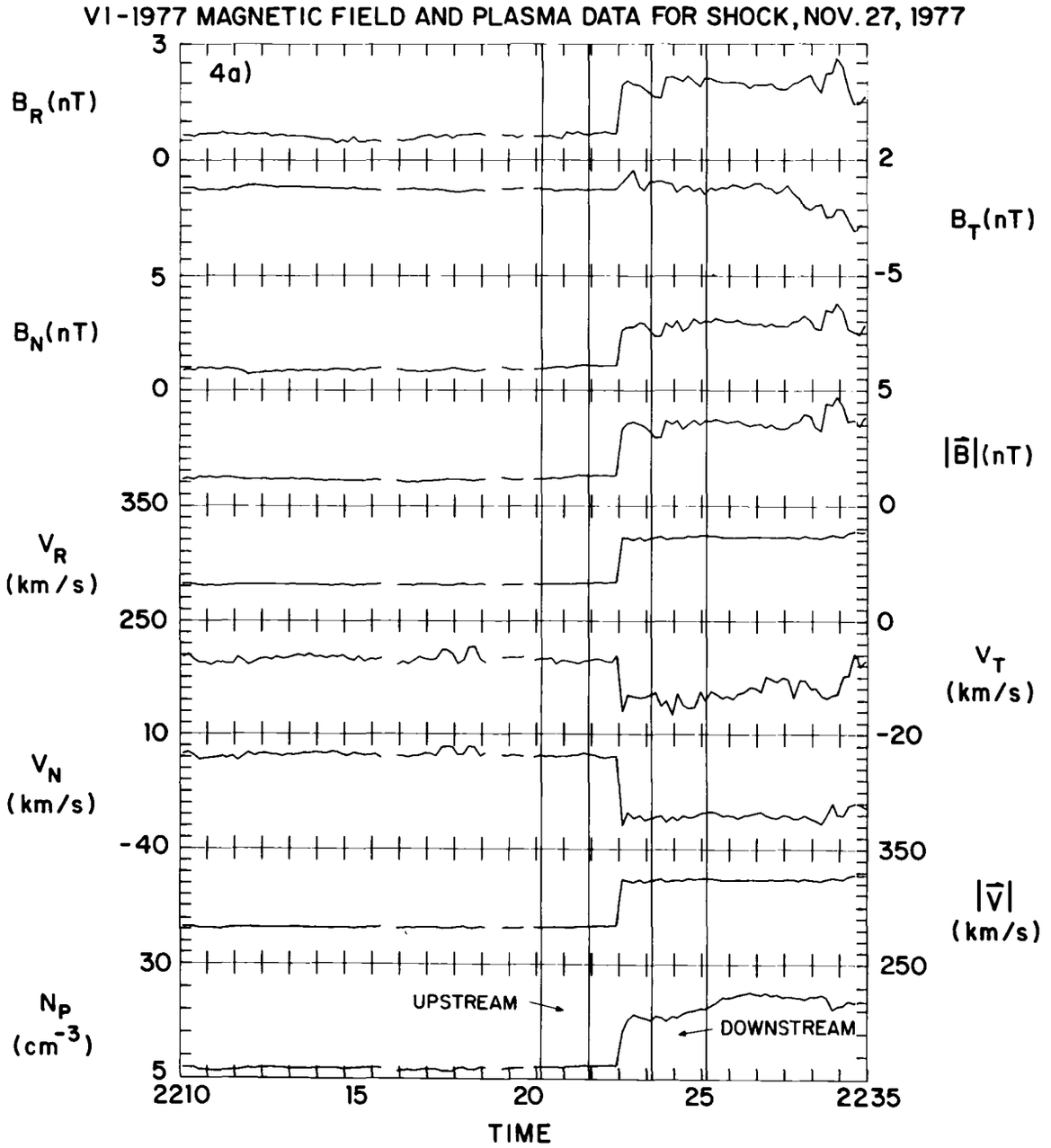

Figure 4a. Plasma and magnetic field data time plots for a real quasi-perpendicular interplanetary shock seen by the Voyager 1 spacecraft. The vertical lines represent the data interval selected for the shock geometry analysis.

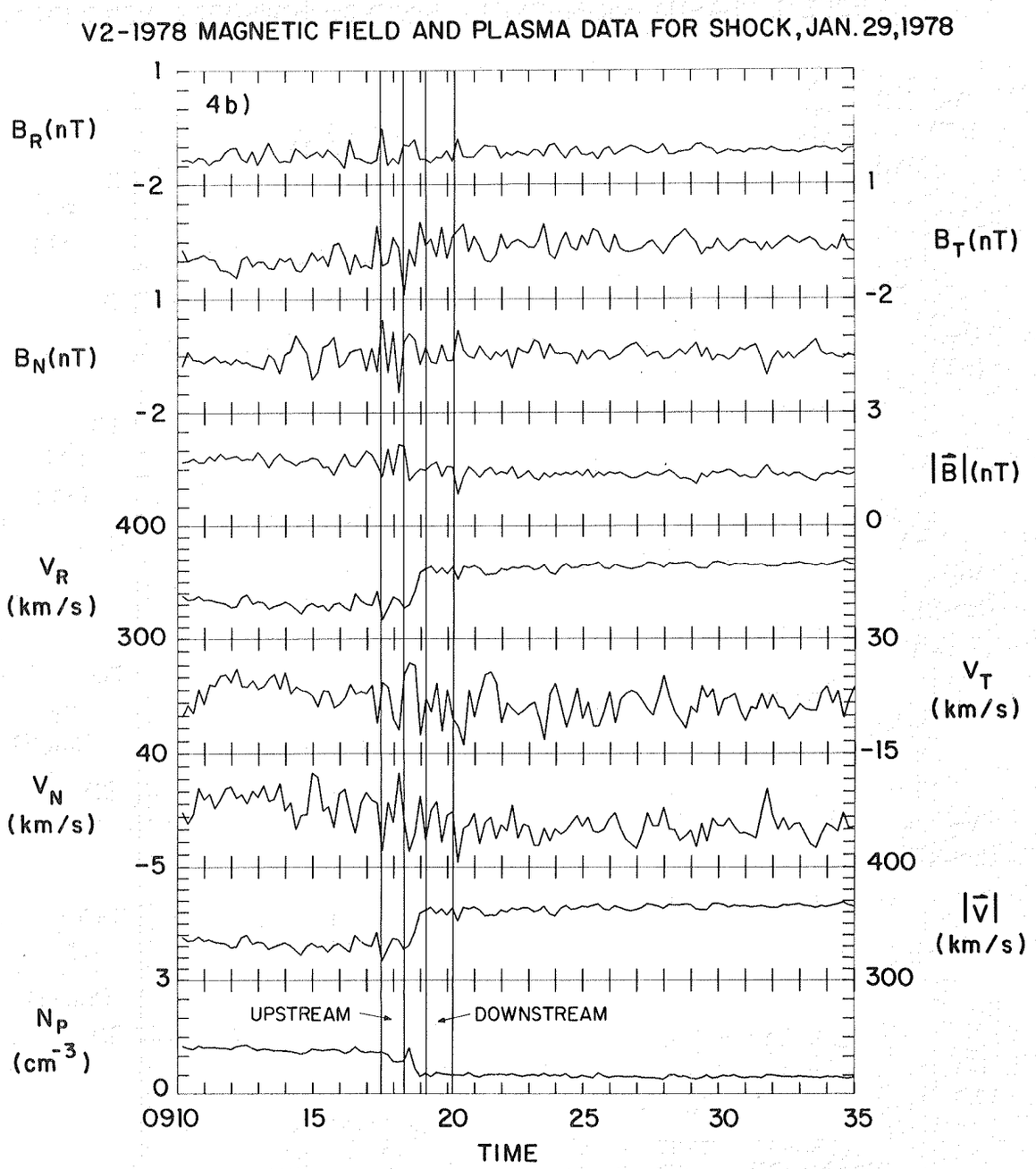

Figure 4b. Plasma and magnetic field data time plots for a real quasi-parallel interplanetary shock seen by the Voyager 2 spacecraft. The vertical lines represent the data interval selected for the shock geometry analysis.

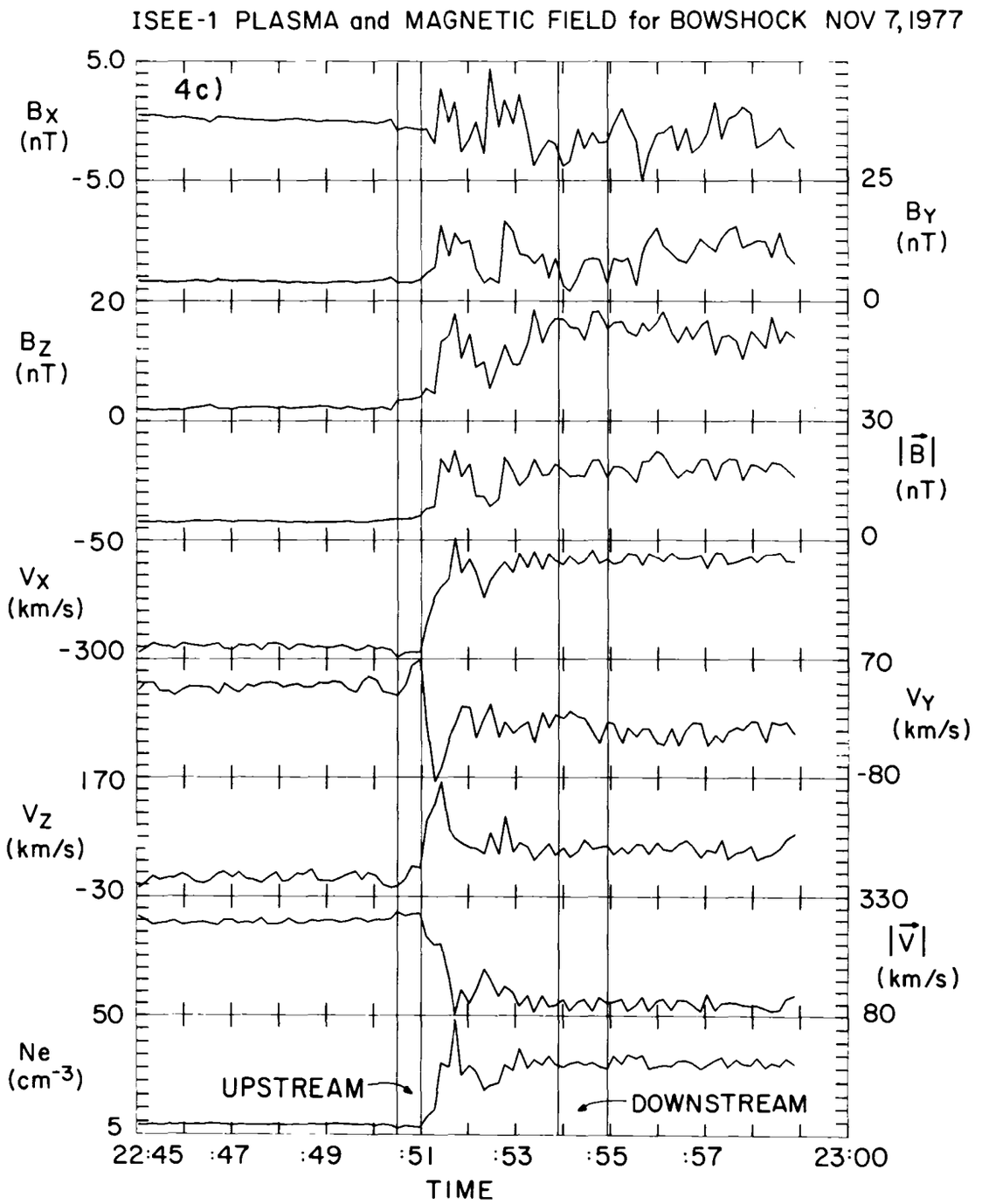

Figure 4c. Plasma and magnetic field data time plots for a real planetary bow shock seen by the ISEE-1 spacecraft. The vertical lines represent the data interval selected for the shock geometry analysis.

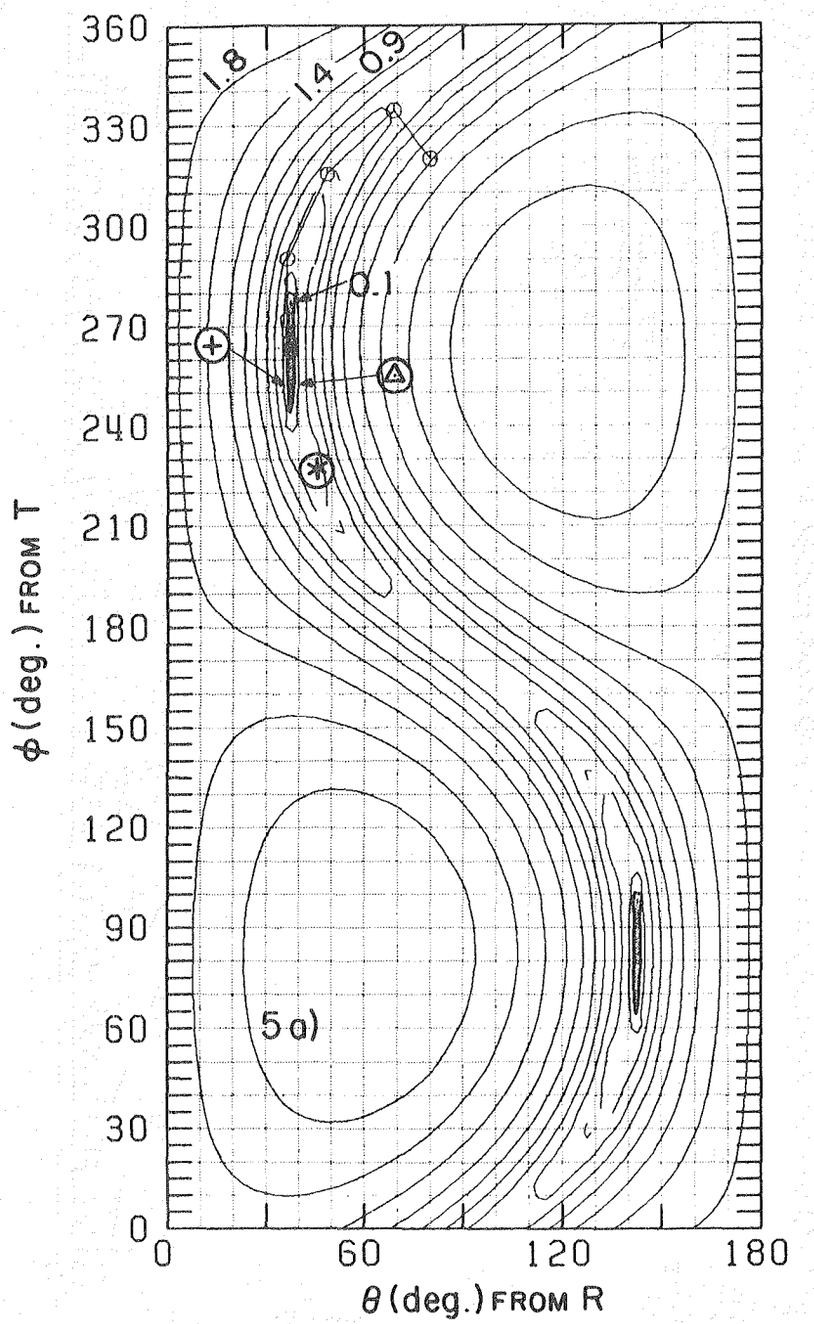

Figure 5a. 'Uniqueness' contour plots of the log χ^2 (θ, ϕ) function versus the shock normal polar angles (θ, ϕ) of a real quasi-perpendicular interplanetary shock. The location of the solution of magnetic coplanarity (MC) '*', velocity coplanarity (VC) '+', Abraham-Shrauner (AS) 'Δ', Lepping-Argentiero (LA) '□' and our solution (VS) '●' are indicated.

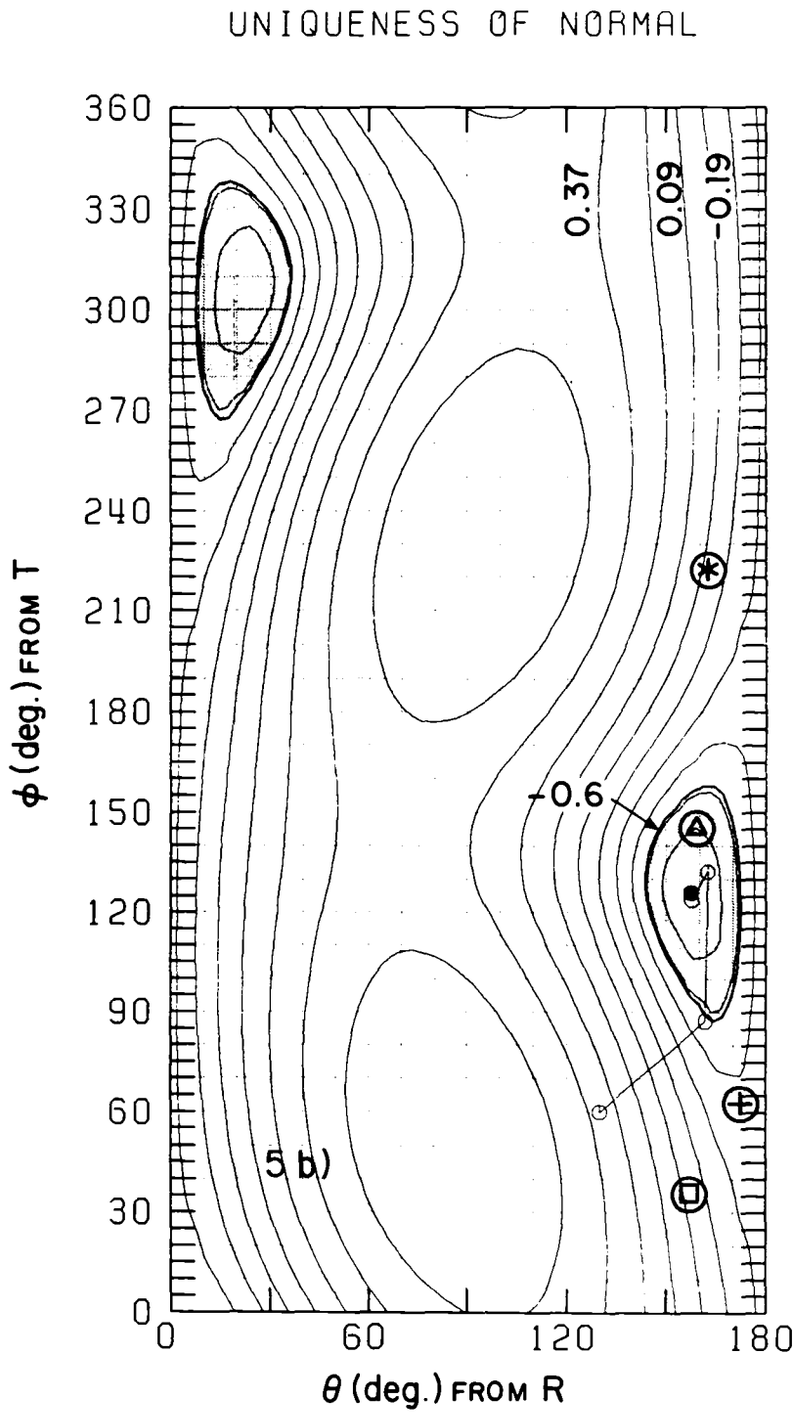

Figure 5b. 'Uniqueness' contour plots of the log χ^2 (θ, ϕ) function versus the shock normal polar angles (θ, ϕ) of a real quasi-parallel interplanetary shock. The location of the solution of magnetic coplanarity (MC) '*', velocity coplanarity (VC) '+', Abraham-Shrauner (AS) 'Δ', Lepping-Argentiero (LA) '□' and our solution (VS) '●' are indicated.

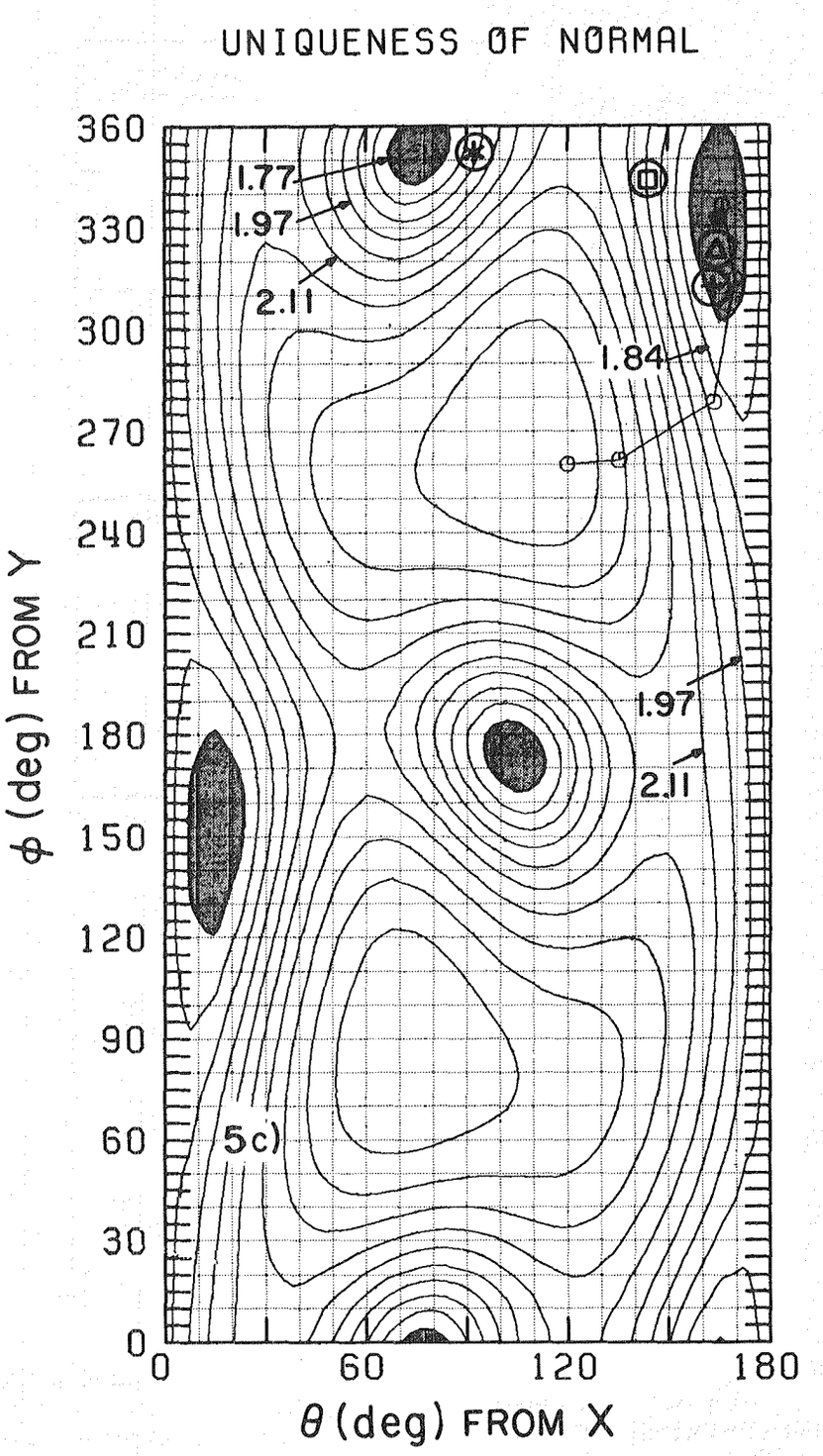

Figure 5c. 'Uniqueness' contour plots of the log χ^2 (θ, ϕ) function versus the shock normal polar angles (θ, ϕ) of a real planetary bow shock. The location of the solution of magnetic coplanarity (MC) '*', velocity coplanarity (VC) '+', Abraham-Shrauner (AS) 'Δ', Lepping-Argentiero (LA) '□' and our solution (VS) '●' are indicated.

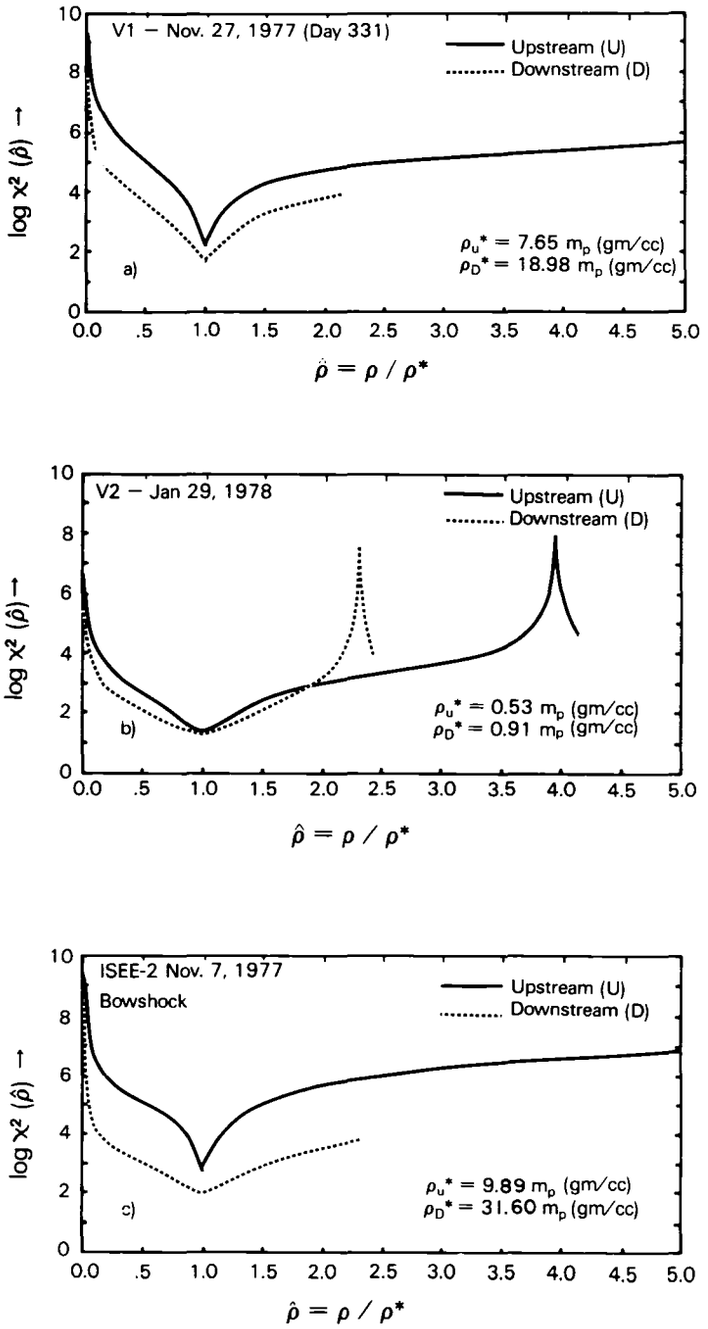

Figure 6. 'Uniqueness' plots of the log χ^2 ($\hat{\rho}$) function versus the normalized density $\hat{\rho} = \rho/\rho^*$ of a real a) quasi-perpendicular and b) quasi-parallel interplanetary shocks and c) planetary bow shock. The normalization constant ρ^* is the value of the asymptotic density obtained by the iterative gradient scheme at the minimum of of the χ^2 function for each side of the shock. Furthermore, the plots on panel b show 'peaks' located at $\hat{\rho} = 3.9$ and 2.3 for the upstream and downstream sides of the shock corresponding to the singularity $\rho = 4\pi G_n^{\ 2}/B_n^{\ 2}$ associated with tangential, contact or rotational discontinuities.

Table 2a. Results of the analysis of the November 27, 1977 interplanetary shock.

		PRE-AVERAGED METHODS			ITERATIVE SCHEMES	
	Sigmas ±σ	Magnetic Coplanarity MC(*)	Velocity Coplanarity VC(+)	Abraham-Shrauner AS(Δ)	Lepping-Argentiero LA(□)	Vinas-Scudder VS(⊕)
θ_{Bn}(deg)	-	84.0	86.8	84.3	-	84.2
V_s(Km/s)	-	288.0	313.9	306.6	-	305.5
δV_s(Km/s)	-	-	-	-	-	±19.3
$\hat{n}_R$	-	0.7370	0.8221	0.7954	-	0.7934
$\hat{n}_T$	-	-0.4593	-0.1456	-0.1509	-	-0.0793
$\hat{n}_N$	-	-0.4959	-0.5519	-0.5869	-	-0.6036
$\delta\Omega_n$(deg)	-	-	-	-	-	±9.0
M_A	-	8.0	8.5	8.5	-	8.0
ΔP(ev/cc)	-	258.2	291.0	291.0	-	295.8
n_1(part/cc)	0.20	7.64	7.64	7.64	-	7.65
V_{R1}(Km/s)	0.40	282.2	282.2	282.2	-	282.8
V_{T1}(Km/s)	0.40	-7.1	-7.1	-7.1	-	-8.8
V_{N1}(Km/s)	0.50	0.8	0.8	0.8	-	2.0
B_{R1}(nT)	0.10	0.64	0.64	0.64	-	0.68
B_{T1}(nT)	0.10	0.20	0.20	0.20	-	0.20
B_{N1}(nT)	0.10	1.02	1.02	1.02	-	1.09
n_2(part/cc)	0.90	18.96	18.96	18.96	-	18.98
V_{R2}(Km/s)	0.90	322.2	322.2	322.2	-	321.6
V_{T2}(Km/s)	1.40	-14.2	-14.2	-14.2	-	-12.6
V_{N2}(Km/s)	1.10	-26.1	-26.1	-26.1	-	-27.2
B_{R2}(nT)	0.20	1.96	1.96	1.96	-	1.85
B_{T2}(nT)	0.30	0.46	0.46	0.46	-	0.47
B_{N2}(nT)	0.30	2.74	2.74	2.74	-	2.58
No. iter	-	-	-	-	$>10^3$	9
T_c (sec)	-	-	-	-	$>10^4$	333.5

Table 2b. Results of the analysis of the January 29, 1978 interplanetary reverse shock.

		PRE-AVERAGED METHODS			ITERATIVE SCHEMES	
	Sigmas ±σ	Magnetic Coplanarity MC(•)	Velocity Coplanarity VC(+)	Abraham-Shrauner AS(Δ)	Lepping-Argentiero LA(□)	Vinas-Scudder VS(⊙)
θ_{Bn}(deg)	-	1.2	36.8	30.8	9.1	29.3
V_s(Km/s)	-	-259.7	-283.8	-270.5	-271.9	-260.8
δV_s(Km/s)	-	-	-	-	-	±39.0
$\hat{n}_R$	-	-0.8666	-0.9936	-0.9434	-0.9392	-0.9248
$\hat{n}_T$	-	-0.3746	0.0548	-0.2741	-0.2750	-0.2231
$\hat{n}_N$	-	-0.3297	0.0990	0.1867	-0.2054	0.3080
$\delta\Omega_n$(deg)	-	-	-	-	-	±18.3
M_A	-	1.3	1.6	1.5	-	1.7
ΔP(ev/cc)	-	7.9	12.5	11.0	10.7	6.8
n_1(part/cc)	0.04	0.53	0.53	0.53	0.53	0.53
V_{R1}(Km/s)	2.9	360.7	360.7	360.7	-	357.4
V_{T1}(Km/s)	7.5	4.9	4.9	4.9	-	6.0
V_{N1}(Km/s)	7.2	12.9	12.9	12.9	-	6.0
B_{R1}(nT)	0.15	-1.29	-1.29	-1.29	-1.29	-1.19
B_{T1}(nT)	0.34	-0.59	-0.59	-0.59	-0.58	-0.58
B_{N1}(nT)	0.23	-0.49	-0.49	-0.49	-0.43	-0.20
n_2(part/cc)	0.12	0.95	0.95	0.95	0.94	0.91
V_{R2}(Km/s)	7.70	328.4	328.4	328.4	-	332.8
V_{T2}(Km/s)	9.63	6.70	6.70	6.70	-	5.70
V_{N2}(Km/s)	11.40	16.2	16.2	16.2	-	25.5
B_{R2}(nT)	0.41	-1.14	-1.14	-1.14	-1.10	-1.33
B_{T2}(nT)	0.60	-1.02	-1.02	-1.02	-1.00	-0.99
B_{N2}(nT)	0.80	-0.38	-0.38	-0.38	-0.73	-0.91
No. iter	-	-	-	-	10	6
T_c (sec)	-	-	-	-		488.2

Table 2c. Results of the analysis of the planetary bowshock.

		PRE-AVERAGED METHODS			ITERATIVE SCHEMES	
	Sigmas ±σ	Magnetic Coplanarity MC(*)	Velocity Coplanarity VC(+)	Abraham-Shrauner AS(Δ)	Lepping-Argentiero LA(□)	Vinas-Scudder VS(⊕)
θ_{Bn}(deg)	-	50.5	83.3	80.8	63.2	74.4
V_s(Km/s)	-	-31.2	-15.2	-11.5	64.5	-8.4
δV_s(Km/s)	-	-	-	-	-	±30.6
$\hat{n}_x$	-	-0.0126	-0.9513	-0.9608	-0.7829	-0.9654
$\hat{n}_y$	-	0.9906	0.2117	0.2195	0.5980	0.2321
$\hat{n}_z$	-	-0.1361	-0.2242	-0.1694	-0.1718	-0.1188
$\delta\Omega_n$(deg)	-	-	-	-	-	±20.4
M_A	-	2.0	8.1	8.1	-	8.1
ΔP(ev/cc)	-	-234.8	5680.0	5700.0	1369.4	5679.8
n_1(part/cc)	0.63	9.89	9.89	9.89	8.10	9.89
V_{x1}(Km/s)	5.90	-289.6	-289.6	-289.6	-	-290.5
V_{y1}(Km/s)	19.43	41.2	41.2	41.2	-	42.8
V_{z1}(Km/s)	17.00	2.3	2.3	2.3	-	11.8
B_{x1}(nT)	0.12	-0.63	-0.63	-0.63	-0.95	-1.27
B_{y1}(nT)	0.04	3.91	3.91	3.91	3.90	2.97
B_{z1}(nT)	0.12	3.58	3.58	3.58	3.66	4.17
n_2(part/cc)	0.76	31.60	31.60	31.60	29.63	31.60
V_{x2}(Km/s)	7.13	-94.3	-94.3	-94.3	-	-93.3
V_{y2}(Km/s)	3.95	-2.3	-2.3	-2.3	-	-3.2
V_{z2}(Km/s)	11.46	48.4	48.4	48.4	-	38.3
B_{x2}(nT)	1.26	-2.40	-2.40	-2.40	1.71	-1.04
B_{y2}(nT)	2.98	5.57	5.57	5.57	10.62	8.78
B_{z2}(nT)	1.38	15.77	15.77	15.77	14.93	13.72
No. iter	-	-	-	-	25	7
T_c (sec)	-	-	-	-	3000.	10.

Table 2c) gives 5679.8 ev/cc which has about 15% deviation from the observed value. This discrepancy can be explained by considering the errors incurred in the evaluation of the predicted pressure, since its calculation depends mostly in the poorly determined asymptotic magnetofluid variables. A crude estimate of the error bounds in the pressure jump due to uncertainties in the asymptotic magnetofluid variables yield ±970 ev/cc. It is clear then, that the predicted pressure jump encompasses within this uncertainty the observed pressure jump across the shock. Scudder et al. [1985] have also reported the pressure jump using a somewhat larger data interval. Their results are consistent within the error bounds to the values reported in this paper.

5. Summary and Conclusions

We have presented and demonstrated the utility of a new, fast, iterative method to determine the geometrical characteristics of a shock using the plasma and magnetic field observations together with a subset of a Rankine-Hugoniot model equations. The method exploited a new vector space that is separable, and unlike other methods contains a smaller number of non-linear unknown variables. An important aspect of the procedure is that 'uniqueness' (or lack thereof) of the solutions can be demonstrated by either analytical or by graphical methods. To the best of our knowledge, this is the first time that 'uniqueness' has been demonstrated for the shock geometry solution. In so doing we also have illustrated the possible ways in which higher order non-linear techniques can obtain a misleading solution.

The analysis we have presented indicates that, unlike extant methods,

this new iterative scheme is reliable at all θ_{Bn}-angles regardless of the shock strength, geometry and direction of propagation relative to the ambient flow. The results in Tables 1a-c and 2a-c for synthetic and real shocks respectively, demonstrate the reliability and accuracy of the method in comparison to other procedures. A virtue of this method which indicates the well-conditioning of the approach is the lack of singular behavior for the extreme situations such as the purely perpendicular ($\theta_{Bn} = 90°$) and parallel ($\theta_{Bn} = 0°$) shock. Our analysis also indicates that the uncertainties in each set of parameters in the least squares sequence is smaller for the shock normal polar angles (i. e. the shock normal $\hat{n}$) and increases for the specification of the asymptotic magnetofluid variables. This implies that the determination of the asymptotic states is more sensitive to errors in the observations. On the other hand, techniques such as magnetic coplanarity, velocity coplanarity and the Abraham-Shrauner mixed data pre-averaged methods select a priori these states to determine the shock normal and in doing so their shock normal calculation will be equally affected by these uncertainties.

The comparison of shock parameters as obtained by different techniques indicates that some of the other methods are reliable for particular shock geometries. In the case of perpendicular shocks, Abraham-Shrauner (AS) and velocity coplanarity (VC) methods gives good results for the shock geometry. On the other hand, magnetic coplanarity (MC) cannot describe the shock geometry of perpendicular shocks since its expression is singular as θ_{Bn} approaches 90°. Similarly the Lepping and Argentiero method cannot reasonably converge for even quasi-perpendicular shocks because its solution depends on the nearly singular expression of magnetic coplanarity. For parallel shocks we find that neither the MC, the LA nor the AS methods can

determine an accurate shock geometry. Again, this is because these methods are singular as θ_{Bn} approaches 0°. Generally all the techniques give reasonably good results for oblique shocks except for the approximate VC method which was demonstrated to fail in this geometry when the flow velocity was not aligned with the shock normal vector.

There still remains various aspects on the determination of the shock geometry which deserve some consideration, however they can be difficult to implement. From the point of view of non-linear optimization, it is possible to incorporate the expression of the scalar pressure jump condition, even in the absence of temperature measurements, into the least squares normal equation for the shock normal polar angles determination. This condition will act as a constraint or penalty function and its effect will be to eliminate some of the unphysical solutions of the problem. Unfortunately, the analytical representation of this penalty function is not clear.

An important application that resulted from our solution is the determination of various frames of references, such as the deHoffman-Teller frame (HTF) [deHoffman and Teller, 1950] and the normal incidence frame (NIF) since their calculation depends on the shock normal, speed, conservation constants and the asymptotic magnetofluid states [Scudder et al., 1985]. With the availability of a technique that determines the optimal conserved fluxes at the shock, there is now a viable way to estimate these quantities which heretofore were expressed as functionals of the poorly determined θ_{Bn} values. For example, the deHoffman-Teller transformation velocity can be written either as

$$\vec{V}_{HT} = -\vec{V}^{*} \cdot \vec{n} \tan\theta_{Bn1} \hat{z}$$

or as

$$\vec{V}_{HT} = c \frac{\vec{E}_t \times \vec{n}}{B_n}$$

in terms of the conserved quantities of higher quality than the state variables.

Appendix A

The analysis of the non-linear system of equations, such as for instance the Rankine-Hugoniot conservation equations (8) - (11), is conveniently accomplished by means of the generalized inverse method. The application of this method to non-linear systems has been previously discussed, e.g. Jackson [1972], Bard [1974] and Lanczos [1961]. The generalized inverse method is a matrix formulation of the least squares problem where the fundamental equation to be solved is represented as

$$\underline{\underline{A}}\, \Delta\vec{p} = \Delta\vec{Y} \tag{A1}$$

where $\Delta\vec{Y} = \vec{Y} - \vec{F}(\vec{x}_i; \vec{p}_j^{(o)})$ is a vector of length N' (i. e. i= 1, N') representing the difference between the observations $\vec{Y}$ and the model prediction and $\underline{\underline{A}}$ is a matrix N' × M formed by the partial derivatives (i. e. the Jacobian) of the model equations with respect to the model unknown parameters $\vec{p}_j$ (i. e. j = 1, M) evaluated at the initial guess.

The solution of the normal equation (A1) is equivalent to the least squares minimization method of the objective $\chi^2(\vec{p})$ (i.e. the chi-square) function. This function is generally defined as

$$\chi^2(\vec{p}) = \sum_{i=1}^{N'} \frac{1}{\sigma^2} (\vec{Y}_i - \vec{F}_i(\vec{x}_i; \vec{p}_j))^2 \tag{A2}$$

where σ represents the standard deviation of the observations. Equation (A2) gives a measure of how well the model equations represented by $\vec{F}(\vec{x}_i; \vec{p}_j)$ fits the observations indicated by the vector $\vec{Y}_i$. In the matrix formalism, the minimization of the χ^2 function is analogous to the

determination of the optimum parameters that minimize the function

$$\chi^2(\vec{p}) = \vec{r}^T \vec{r} \tag{A3}$$

where $\vec{r}$ is the residual vector given by $\vec{r} = (\underline{\underline{A}}\ \Delta\vec{p} - \Delta\vec{Y})$ and $\vec{r}^T$ is the transpose vector. Generally, the objective function χ^2 is normalized by the number of degrees of freedom ν of the system. The number of degrees of freedom is defined as the difference between the total number of data points N' and the number of unknown parameters per model equation (M/L) (i. e. ν = N' - M/L). Since the minimization of equation (A3) and the generalized method solution of equation (A1) have been shown to be mathematically equivalent [Lanczos, 1961; Jackson, 1972; Bard, 1974] we shall instead proceed with the application of the later method to the linearized matrix equation (A1). The reader is refered to the mentioned papers (and references therein) for the theoretical aspects of these methods.

The matrix formulation of the generalized inverse method utilizes the singular value decomposition of Lanczos [Lanczos, 1961; Jackson, 1972]. This approach requires the estimation of the eigenvalues and eigenvectors associated with the matrix $\underline{\underline{A}}$ in (A1). This approach is convenient when the matrix $\underline{\underline{A}}$ is well conditioned in the sense that its eigenvalues are large and the iteration scheme will require short steps in the parameter space, keeping the linearization well inside its region of validity. However, if the matrix $\underline{\underline{A}}$ is close to being ill-conditioned, which implies that some of its eigenvalues are zero or numerically very small, the solution vector $\Delta\vec{p}$ will take large steps in the parameter space that may well be outside of the region where the linearization is appropriate. This iterative process may then diverge unless some method of limiting the iterative step size is

employed. Two generally recognized options are used in this case. One option requires constructing a solution from the contribution of only the larger eigenvalues as suggested by Lanczos [1961] and Jackson [1972]. Although this procedure is reasonably appropriate, it requires the monitoring of the eigenvalues at each step in the iteration process making it slow. A second option, that we consider more practical and that can be easily implemented is to follow the technique known as the Marquardt-Levenberg's algorithm [Levenberg, 1944; Marquardt, 1963; Bard, 1974; Lawson and Hanson, 1974]. With this method the stability of the iterative procedure is improved by limiting the step size (more sensitive in the direction corresponding to the small eigenvalues) by introducing what is known as a "cut-off" eigenvalue or Marquardt parameter α^2. Furthermore, with this "cut-off" eigenvalue, fast and accurate convergence is invoked and the need to monitor the small eigenvalues at each step of the iteration is avoided.

The solution, then, of equation (A1) is now given by

$$\Delta\vec{p}^{*} = \underline{\underline{A}}_{g}^{-1} \Delta\vec{Y} \tag{A4}$$

where $\underline{\underline{A}}_{g}^{-1}$ is the generalized inverse defined by

$$\underline{\underline{A}}_{g}^{-1} = (\underline{\underline{H}} + \alpha^2 \underline{\underline{B}})^{-1} \underline{\underline{A}}^{T} \tag{A5}$$

where $\underline{\underline{A}}^{T}$ is the transpose matrix, $\underline{\underline{H}} = \underline{\underline{A}}^{T} \underline{\underline{A}}$ is the approximate Hessian matrix which is positive definite and of size M x M, $\underline{\underline{B}}$ is a diagonal matrix whose elements coincide with the diagonal elements of $\underline{\underline{H}}$ if $H_{ii} \neq 0$ and with the unit matrix $\underline{\underline{I}}$ if $H_{ii} = 0$. The parameter α^2 is the Marquardt parameter and

its size controls not only the step size but also the contribution of the small eigenvalues to the solution at each iteration step.

In general the quantities in the vector $\vec{F}_i(\vec{x}_i; \vec{p}_j)$ represent entities having different physical dimensions. For example, in the shock normal case in section 3a the function $\vec{F}_i(\vec{x}_i; \vec{p}_j)$ is a vector of seven components representing the normal component of the magnetic field, the components of the tangential momentum flux and electric field in an arbitrary coordinate system. Since these quantities are constructed from the magnetic field and plasma observations, it is clear that some of the observations may be known to be less reliable than others, and we want to be certain that our parameter estimates will be less influenced by those than by the more accurate ones. For this reason it is convenient to weight equation (A1) before the parameters are estimated. After all, we cannot escape from the statistical nature of the observed data. One way of weighting the system of equations (A1) is by constructing the standard deviations associated with the physical variables of the Rankine-Hugoniot system. If the observations are statistically independent we define a diagonal matrix $\underline{\underline{W}} = (1/\sigma_i)$ of size $N' \times N'$ from the standard deviations. Operating on the normal equation (A1) we have the solution

$$\Delta\vec{p}^{*} = (\underline{\underline{A}}^T \underline{\underline{W}}^T \underline{\underline{W}} \underline{\underline{A}} + \alpha^2 \underline{\underline{B}})^{-1} \underline{\underline{A}}^T \underline{\underline{W}}^T \underline{\underline{W}} \Delta\vec{Y} \qquad \text{(A6)}$$

At this point the χ^2 function can be generalized to be $\chi^2 = \vec{r}^T \underline{\underline{W}}^T \underline{\underline{W}} \vec{r}$.

Let us now address the problem of the reliability and precision of the model parameters. It is not enough to compute a vector solution $\vec{p}^{*}$ without a simultaneous estimate of the error bounds in the parameters determined.

One way of expressing the reliability of the solution is by constructing what is called the resolution matrix [Lanczos, 1961; Jackson, 1972] given by

$$\underline{\underline{R}} = \underline{\underline{A}}_g^{-1} \underline{\underline{A}}$$

The degree to which the $\underline{\underline{R}}$ matrix approximates the identity matrix is a measure of the resolution obtainable from the data for each parameter. If the matrix $\underline{\underline{R}}$ is nearly diagonal, then each parameter is a weighted sum of the others.

To estimate the error bounds on the obtained parameters $\vec{p}^*$, it is necessary to assume a statistical uncertainty distribution for them. This kind of test are exact only if the measurement errors do indeed follow such a distribution. Since in general such a distribution is unknown, a more practical way of obtaining the error bounds in the parameter space is to consider the departure of the objective (risk) function $\chi^2(\vec{p})$ from the obtained optimal value $\chi^2(\vec{p}^*)$ [Bard, 1974] as follows

$$|\chi^2(\vec{p}) - \chi^2(\vec{p}^*)| \leq \varepsilon \qquad \text{(A7)}$$

where ε is the largest difference that one is willing to consider insignificant (i. e. the indifference region). Therefore we have no reason to prefer $\vec{p}^*$ over any other value of $\vec{p}$ for which (A7) is satisfied. The region enclosed in (A7) is named the indifference region. In a small neighborhood of $\vec{p}^*$ we can now approximate $\chi^2(\vec{p})$ by a Taylor series expansion

$$\chi^2(\vec{p}) \simeq \chi^2(\vec{p}^*) + \vec{q}^{*T}\, \delta\vec{p} + \frac{1}{2}\, \delta\vec{p}^T\, \underline{\underline{H}}^*\, \delta\vec{p} \qquad \text{(A8)}$$

where $\delta\vec{p} = \vec{p} - \vec{p}^*$, and $\vec{q}^*$ and $\underline{\underline{H}}^*$ are the gradient vector and the Hessian

matrix of the χ^2 function respectively, evaluated at $\vec{p} = \vec{p}^*$. If $\vec{p}^*$ is an optimal extremum of $\chi^2(\vec{p})$, then $\vec{q}^*$ must vanish. We can now answer the question of the error bounds in the parameter $\vec{p}$ because equation (A8) properly written represents an M-dimensional ellipsoid whose principal axes (or eigenvalues of $\underline{\underline{H}}$) are a measure of these errors. Note that equation (A8) can now be written as

$$\delta\vec{p}^T \underline{\underline{H}}^* \delta\vec{p} \leq 2\varepsilon \tag{A9}$$

This is easily seen by noticing that equation (A9) can be formulated as an eigenvalue problem of the form

$$\underline{\underline{H}}^* \delta\vec{p} = \underline{\underline{\Lambda}} \delta\vec{p}$$

where $\underline{\underline{\Lambda}}$ ia a diagonal matrix of the eigenvalues of $\underline{\underline{H}}^*$. Thus operating by $\delta\vec{p}^T$ at both sides of this equation and using (A9) we get

$$\delta\vec{p}^T \underline{\underline{\Lambda}} \delta\vec{p} = 2\varepsilon \tag{A10}$$

Equation (A10) states that the length of each vector component of $\delta\vec{p}$ is proportional to $\sqrt{(2\varepsilon/\lambda)}$ where λ is its corresponding eigenvalue and the eigenvector represents the principal axis of the multidimensional ellipsoid. The largest axis (smallest eigenvalue) defines the worst-determined direction in $\vec{p}$ space and the shortest axis (largest eigenvalue) defines the best determined direction. Thus the solution of (A10) gives a reliable measure of the errors in the parameter determined.

In a different way, if one does not have a good measure of the

indifference region ε, it is possible to adopt an 'ad hoc' error distribution, such as for example, the normal distribution and determine the confidence region ε for $\vec{p}^{*}$ provided that the covariance matrix $\underline{\underline{C}}$ of the errors of the observations is known [Bard, 1974; Jackson, 1972; Scheffé, 1959].

Acknowledments. We thank H. S. Bridge, N. F. Ness, K. W. Ogilvie and C Russell, principal investigators of the Voyager and ISEE-1 plasma and magnetic field experiments, respectively, for permission to use the plasma and magnetic field data. We would especially like to express our appreciation to R. Lepping and M. Acuña for the many stimulating discussions, their support and for allowing us to make use of their algorithm. We are greatful to E. Sittler for supplying the Voyager electron information and to Y. C. Whang for allowing us to use his shock algorithm. We also thank L. Burlaga, A. Lazarus and M. Goldstein for their continuous support.

References

Abraham-Shrauner, B., Determination of magnetohydrodynamic shock normals, J. Geophys. Res., 77, 736, 1972.

Abraham-Shrauner, B. and S, H. Yun, Interplanetary shocks seen by Ames plasma probe on Pioneer 6 and 7, J. Geophys. Res., 81, 2097, 1976.

Acuña, M. H. and R. P. Lepping, Modification to shock fitting program, J. Geophys. Res., 89, 11004, 1984.

Akhiezer, A. I., I. A. Akhiezer, R. V. Polovin, A. G. Sitenko and K. N. Stepanov, Plasma Electrodynamics: Linear Theory, Vol. I, Pergamon Press, New York, 1975.

Armstrong, T. P., M. E. Pesses and R. B. Decker, Shock drift acceleration, in Collisionless Shock Waves in the Heliosphere, edited by E. C. Stone and B. Tsurutani, AGU Geomonograph, in press, 1985.

Bard, Y., Nonlinear Parameter Estimation, Academic Press, New York, 1974.

Boyd, T. J. and J. J. Sanderson, Plasma Dynamics, Barnes and Noble Inc., New York, 1969.

Burlaga, L. F., Hydromagnetic waves and discontinuities in the solar wind, Spac. Sci. Rev., 12, 600, 1971.

Chao, J. K., Interplanetary Collisionless Shock Waves, Rep. CSR TR-70-3, Massachusetts Institute of Technology, Cambridge, Mass., 1970.

Chao, J. K. and K. C. Hsieh, On determining magnetohydrodynamic shock parameters θ_{Bn} and M_A, Planet. Space Sci., 32, 641, 1984.

Colburn, D. C. and C. P. Sonett, Discontinuities in the solar wind, Space Sci. Rev., 5, 439, 1966.

deHoffman, F. and E. Teller, Magnetohydrodynamic shocks, Phys. Rev., 80, 692, 1950.

Edminston, J. P. and C. F. Kennel, A parametric survey of the first critical Mach number for fast MHD shock, J. Plasma Phys., 32, 429, 1985.

Forman, M. A. and G. M. Webb, Acceleration of energetic particles, in Collisionless Shock Waves in the Heliosphere, edited by E. C. Stone and B. Tsurutani, AGU Geomonograph, in press, 1985.

Goodrich, C. C. and J. D. Scudder, The adiabatic energy change of plasma electrons and the frame dependence of the cross-shock potential at collisionless magnetosonic shock waves, J. Geophys. Res., 89, 6654, 1984.

Gosling, J. T., M. F. Thomsen, S. J. Bame, W. C. Feldman, G. Paschmann and N. Sckopke, Evidence for specularly reflected ions upstream from quasi-parallel bow shock, Geophys. Res. Lett., 9, 1333, 1982.

Greenstadt, E., V. Formisano, C. Goodrich, J. T. Gosling, M. Lee, M. Leroy, M. Mellot, K. Quest, A. E. Robson, P. Rodriguez, J. Scudder, J. Slavin, M. Thomsen, D. Winske and C. S. Wu, Collisionless Shock Waves in the Solar Terrestrial Enviroment, Solar Terrestrial Physics: Present and Future, edited by D. M. Butler and K. Papadopoulos, NASA publication 1120, 1984.

Jackson, D. D., Interpretation of Innacurate, Insufficient and Inconsistent data, Geophys. J. R. Astr. Soc., 28, 97, 1972.

Kennel, C. F., J. P. Edminston and T. Hada, A quarter century of collisionless shock research, in Collisionless Shock Waves in the Heliosphere, edited by E. C. Stone and B. Tsurutani, AGU Geomonograph, in press, 1985.

Lanczos, C., Linear Differential Operators, D. Van Nostrand, Princeton, N. J., 1961.

Landau, L. D. and E. M. Lifshitz, Electrodynamic of Continuous Media,

Pergamon Press, pp 224-233, New York, 1960.

Lawson, C. L. and R. J. Hanson, Solving Least Squares Problems, Prentice Hall Inc, New Jersey, 1974.

Lepping, R. P. and P. D. Argentiero, Single spacecraft method of estimating shock normals, J. Geophys. Res., 76, 4349, 1971.

Lepping, R. P., Influence of thermal anisotropy on best-fit estimates of shock normals, J. Geophys. Res., 77, 2957, 1972.

Levenberg, K., A method for the solution of certain nonlinear problems in least squares, Quart. Appl. Math., 2, 164, 1944.

Marquardt, D. W., An algorithm for least squares estimation of nonlinear parameters, SIAM J., 11, 431, 1963.

Ogilvie, K. W. and L. F. Burlaga, Hydromagnetic shocks in the solar wind, Solar Phys., 8, 422, 1969.

Russell, C. T., M. M. Mellott, E. J. Smith and J. H. King, Multiple spacecraft observations of interplanetary shocks: Four spacecraft determination of shock normals, J. Geophys. Res., 88, 4739,1983a.

Russell, C. T., J. T. Gosling, R. D. Zwickl and E. J. Smith, Multiple spacecraft observations of interplanetary shocks: ISEE three dimensional plasma measurements, J. Geophys. Res., 88, 9941, 1983b.

Scheffé, H., The Analysis of Variance, John Wiley & Sons Inc., New York, 1959.

Scudder, J. D., L. F. Burlaga and E. W. Greenstadt, Scale lengths in quasi-parallel shocks, J. Geophys. Res., 89, 7545, 1984.

Scudder, J. D., C. Lacombe, A. Mageney, C. C. Harvey, J. T. Gosling, G. Paschmann, C. T. Russell, T. L. Aggson and R. Anderson, The resolved layer of a collisionless, high β, supercritical, quasiperpendicular shock wave: geometry, current system and scales, to be submitted to J.

Geophys. Res., 1985.

Sonnerup, B. U. O., Acceleration of particles reflected at a shock front, J. Geophys. Res., 74, 1301, 1969.

Tidman, D. A. and N. A. Krall, Shock Waves in Collisionless Plasmas, John Wiley and Sons Inc., New York, 1971.

Viñas, A. F., M. L. Goldstein and M. H. Acuña, Spectral amalysis of magnetohydrodynamic fluctuations near interplanetary shocks, J. Geophys. Res., 89, 3762, 1984.

Whang, Y. C., F. Fei and H. Du, Transport of interplanetary fluctuations to the magnetopause, submitted to J. Geophys. Res., 1985.

Wu, C. S., A fast Fermi process: Energetic electrons accelerated by a nearly perpendicular bow shock, J. Geophys. Res., 89, 8857, 1984.

A. F. Viñas and J. D. Scudder, Code 692, Laboratory for Extraterrestrial Physics, NASA/Goddard Space Flight Center, Greenbelt, MD, 20771.

BIBLIOGRAPHIC DATA SHEET

1. Report No.	2. Government Accession No.	3. Recipient's Catalog No.
TM-86214		

4. Title and Subtitle	5. Report Date
FAST AND OPTIMAL SOLUTION TO THE 'RANKINE-HUGONIOT PROBLEM'	May 1985
	6. Performing Organization Code

7. Author(s)	8. Performing Organization Report No.
Adolfo F. Viñas, Jack D. Scudder	85BO392

9. Performing Organization Name and Address	10. Work Unit No.
NASA/Goddard Space Flight Center Greenbelt, Maryland 20771	11. Contract or Grant No.
	13. Type of Report and Period Covered
12. Sponsoring Agency Name and Address	Technical Memorandum
	14. Sponsoring Agency Code

15. Supplementary Notes

16. Abstract

A new, definitive, reliable and fast iterative method is described for determining the geometrical properties of a shock (i.e. θ_{Bn}, $\vec{n}$, V_s and M_A), the conservation constants and the self-consistent asymptotic magnetofluid variables, that uses the three dimensional magnetic field and plasma observations. The method is well conditioned and reliable at all θ_{Bn} angles regardless of the shock strength or geometry. Explicit proof of 'uniqueness' of the shock geometry solution by either analytical or graphical methods is given. The method is applied to synthetic and real shocks, including a bow shock event and the results are then compared with those determined by preaveraging methods and other iterative schemes. A complete analysis of the confidence region and error bounds of the solution is also presented.

17. Key Words (Selected by Author(s))	18. Distribution Statement
Rankine-Hugoniot, interplanetary shocks, tangential, rotational, contact discontinuity	Unclassified-Unlimited STAR: #75 and #88

19. Security Classif. (of this report)	20. Security Classif. (of this page)	21. No. of Pages	22. Price*
Unclassified	Unclassified	73	

*For sale by the National Technical Information Service, Springfield, Virginia 22161

GSFC 25-44 (10/77)

End of Document